UNIVERSITAT DE BARCELONA

FACULTAT DE QUÍMICA

DEPARTAMENT DE QUÍMICA FÍSICA

Programa de Doctorat d'Electroquímica: Ciència i Tecnologia

Bienni 2004-2006

L'anoditzat d'alumini com a eina per a la fabricació de nanomaterials 1D

Memòria que presenta Josep M Montero Moreno per optar al títol de Doctor per la Universitat de Barcelona

Directors:

Carlos Müller Jevenois

Catedràtic de Química Física
Universitat de Barcelona

Maria Sarret Pons

Professora titular de Química Física
Universitat de Barcelona

Barcelona, 30 de març de 2009

Capítol 3

Optimització del procés d'anoditzat i caracterització del sistema Al/OAA

Optimització del procés d'anoditzat i caracterització del sistema alumini/òxid anòdic d'alúmina (Al/OAA)

3.1. Introducció al capítol 3

L'estudi presentat en aquest capítol analitza el procés de preparació i la caracterització de membranes d'alúmina porosa mitjançant el doble anoditzat de l'alumini. L'objectiu principal és fabricar capes anòdiques útils per a la fabricació de nanoestructures 1D, per la qual cosa les membranes han de satisfer una sèrie de requisits:

- Presentar una estructura cel·lular hexagonal ben definida: cal que els paràmetres bàsics de l'estructura porosa siguin fàcilment caracteritzables: la distància entre porus (d_{int}), el diàmetre de porus (d_p) i la densitat de porus (δ_p).

- Exhibir una alta homogeneïtat: es busca una elevada regularitat de la distància entre porus i del diàmetre de porus en tota l'estructura, tant en el pla com longitudinalment.

- Mostrar un cert grau d'ordre: interessa que l'estructura es correlacioni el màxim possible a l'estructura idealitzada del rusc d'abella. Es buscaran les condicions òptimes per al creixement de capes auto-ordenades.

- Provar una fàcil controlabilitat: és condicionant que els paràmetres estructurals (d_{int}, d_p, δ_p), el gruix de la capa i el grau d'ordre es defineixin en funció de les condicions d'operació, de manera que es puguin fabricar membranes a la carta.

Per a tal fi, s'ha realitzat un estudi de la influència de diversos paràmetres d'operació en els dos modes bàsics de control de l'anoditzat: control de voltatge (o

potenciostàtic) i control de corrent (o galvanostàtic). En relació al terme potenciostàtic, aclarir que, tot i que s'ha utilitzat indistintament en aquest treball, des d'un punt de vista electroquímic no es pot considerar correcte el seu ús. En general, es parla de procés potenciostàtic si existeix un control real del voltatge aplicat a la interfase electroquímica d'interès (en aquest cas a l'alumini). Això s'aconsegueix introduint un tercer elèctrode de referència i minimitzant la caiguda òhmica de l'electròlit. En aquest estudi, i en general en la investigació del procés d'anoditzat de l'alumini, es treballa amb una cel·la de dos elèctrodes (càtode i ànode) perquè els alts voltatges requerits fan difícil la utilització d'un elèctrode de referència. El voltatge aplicat (controlat) és el corresponent al sistema electroquímic complert (dues interfases i la dissolució). *Strictu sensu*, en aquestes condicions no es pot parlar de control potenciostàtic, encara que la caiguda de potencial majoritària es produeix en la interfase anòdica. No obstant, aquesta asimetria fa que l'ús del terme potenciostàtic quan s'aplica un voltatge constant entre càtode i ànode estigui molt estès, encara que estrictament no sigui correcte la seva aplicació.

Els diferents estudis realitzats han permès extreure una sèrie de resultats sobre el procés d'anoditzat i les membranes d'alúmina anòdica, els quals s'han publicat a diverses revistes científiques adjuntades al final del capítol. Els treballs es centren en quatre aspectes bàsics del procés:

- La condició inicial de la superfície d'alumini, publicat a la revista *Surface and Coatings Technology*, pàgina 57 de la tesi.

- El doble anoditzat en control de voltatge, publicat a la revista *Journal of the Electrochemical Society*, pàgina 65 de la tesi.

- El doble anoditzat en control de corrent, enviat a la revista *Electrochimica Acta*, pàgina 73 de la tesi.

- L'estructura de la capa d'alúmina, publicat a la revista *Materials Chemistry and Physics*, pàgina 81 de la tesi.

3.2. Anàlisi de l'estat superficial de l'alumini previ a l'anoditzat

La primera part del treball analitza la importància de l'estat superficial de l'alumini 1050 abans del procés d'anoditzat, determinant-ne la relació que manté amb el doble anoditzat auto-ordenat. S'ha estudiat l'evolució de l'estat superficial de l'alumini durant les diferents etapes del pretractament fins a arribar a una superfície òptima

per a la realització del doble anoditzat auto-ordenat. S'ha observat que no és possible assolir un grau d'ordenació elevat de la membrana anòdica en un alumini d'aquest tipus sense un pretractament adient, establint-se la necessitat de treballar amb una superfície de molt baixa rugositat i alhora neta de compostos intermetàl·lics o compostos precipitats. Una etapa com l'electropolit de l'alumini esdevé essencial per a la consecució dels objectius marcats anteriorment, però no única, sobretot considerant el grau d'impuresa de l'alumini tractat. Els resultats assenyalen la necessitat de les diverses etapes del pretractament:

- **Desgreixatge alcalí**: elimina restes de greixos i olis incorporats a la superfície durant la manipulació o el procés de fabricació de l'alumini sense damnificar-la (pH ~ 11 - 12) utilitzant una sèrie de tensioactius.

- **Decapat alcalí**: s'aprofita la sensibilitat de l'alumini a les dissolucions alcalines per renovar tota la superfície, eliminant-ne la capa més externa i, en conseqüència, més malmesa. En medis fortament alcalins (pH ~ 13 – 14) es produeix la reacció [3.a].

[3.a] $$Al + 3H_2O + OH^- \rightarrow Al(OH)_4^- + \frac{3}{2}H_2$$

L'addició d'un agent complexant com el gluconat de sodi facilita la incorporació de l'alumini a la dissolució, minimitzant-ne la precipitació, a l'igual que la dels altres metalls presents en l'alumini. De tota manera, és inevitable la precipitació d'aluminats, òxids i hidròxids en aquesta etapa i cal un segon pas de neteja.

- **Decapat àcid I**: en aquesta etapa es dissol el precipitat format durant l'atac alcalí de l'alumini a través de la hidròlisi àcida d'aquests compostos, en general segons les reaccions [3.b] i [3.c].

[3.b] $$M(OH)_n + n\,H^+ \rightarrow M^{n+} + n\,H_2O$$

[3.c] $$M_2O_n + 2n\,H^+ \rightarrow 2\,M^{n+} + n\,H_2O$$

- **Electropolit i decapat àcid II**: en el conjunt de les etapes anteriors la rugositat superficial es redueix en un 50 % (*rms* = 270 nm, mesurat per interferometria de llum blanca), a més d'eliminar els compostos intermetàl·lics i òxids superficials i renovar la superfície per eliminar defectes. De tota manera, el posterior anoditzat demostra que no és un tractament suficient per al desenvolupament de capes d'alúmina estructurades. S'ha comprovat que la posterior reducció de la rugositat a valors d'escala nanomètrica mitjançant el procés de polit electroquímic (*rms* < 80 nm determinada per interferometria de llum blanca i < 10 nm per AFM) permet el creixement de la capa amb un menor número de defectes en l'empaquetament hexagonal de les cel·les. S'ha detectat que el procés d'electropolit utilitzat genera una capa compacta superficial, la qual està íntimament relacionada amb el procés de nucleació dels porus. L'optimització de la capa formada durant l'electropolit (modificant-ne la temperatura del bany) i el posterior atac en dissolució àcida amb ions Cr(VI) permet obtenir una superfície amb una rugositat considerablement homogènia, la qual condueix a capes d'alúmina amb una estructura més desitjable per a l'obtenció de nanomaterials 1D.

D'altra banda, s'ha establert la importància de l'etapa intermèdia de decapat àcid durant el procés del doble anoditzat alhora d'aconseguir una superfície nanotexturada òptima per a la nucleació dels porus en la segona etapa d'anoditzat. L'eliminació complerta de la primera capa d'òxid de forma controlada només es pot assolir seguint uns criteris fixats per tal d'estalviar temps i evitar sobreexposicions de la superfície. En conclusió, es mostra que el doble anoditzat funciona igualment per a un alumini relativament impur (99.5 %), en comparació amb l'alumini d'alta puresa utilitzat comunament (> 99.999 %), si es troba el procés de pretractament adient.

3.3. Comparativa entre els dos modes bàsics d'anoditzat: control en voltatge i control en corrent

3.3.1. Consideracions generals dels processos d'anoditzat en control de voltatge i de corrent

En una segona etapa de l'estudi, s'ha analitzat el procés del doble anoditzat, tant en control de voltatge com de corrent. Els resultats obtinguts es presenten en dues publicacions per separat (pàg. 65 i 73). La comparació dels resultats mostra que, tot i tractar-se de processos molt semblants, la similitud està limitada a les condicions d'operació i al tipus d'alumini utilitzat. Per exemple, en quant al mecanisme de formació, sembla que les etapes de formació de la capa d'alúmina anòdica són les mateixes: I) creixement de la capa compacta; II) ruptura i nucleació dels porus; III) inici del mecanisme de dissolució assistida per camp elèctric i creixement dels porus

(pseudo-estat estacionari); IV) caiguda òhmica produïda per l'engruiximent de la capa. Aquestes etapes es poden seguir en els respectius diagrames voltatge – temps (procés galvanostàtic) i densitat de corrent – temps (procés en control de voltatge). Igualment, s'ha establert que, per a totes les condicions assajades, els gruixos obtinguts només depenen de la càrrega total per unitat d'àrea que s'ha fet passar al llarg de tot el procés, segons la relació lineal [3.d].

[3.d] $$e(\mu m) = 0.45 \cdot Q(C \cdot cm^{-2}) + 0.52, \quad \forall\, c, T, t, V \; i \; j \; assajada$$

D'altra banda, també s'ha observat que la velocitat de creixement de la capa depèn únicament de la densitat de corrent, ja sigui aplicada (anoditzat en control de corrent) o mesurada (anoditzat en control de voltatge), d'acord amb l'equació [3.e].

[3.e] $$v(nm \cdot min^{-1}) = 23.57 \cdot j(mA \cdot cm^{-2}) + 34.90$$

La diferència entre els dos tipus de processos és que la densitat de corrent és fixa per a un procés en control de corrent, però varia amb les condicions experimentals per a un procés en control de voltatge. Per exemple, a la figura 3.1 es mostra la relació entre la densitat de corrent mesurada i la temperatura – concentració del bany per a un procés d'anoditzat en àcid oxàlic i en control de voltatge (45 V – condicions d'auto-ordenació).

Com era d'esperar, majors concentracions i temperatures produeixen majors densitats de corrent, per a un valor de voltatge fix, el que es tradueix en una major velocitat de creixement. Aquest fet està lligat a l'increment de la conductivitat iònica de la dissolució i a l'augment de la cinètica del procés d'oxidació de l'alumini i dissolució de l'alúmina.

Aquests resultats indiquen que les eficiències d'ambdós processos són iguals, sempre i quan les condicions experimentals generin respostes recíproques de voltatge i corrent i sempre dins l'estat estacionari: a una càrrega fixa, s'obté sempre el mateix gruix, independentment del tipus de procés. Aquest fet introdueix un cert grau de llibertat en els processos en control de corrent a l'hora de fixar les condicions de treball, amb el que es pot minimitzar el risc de cremar de les peces més fàcilment i fixar les condicions d'auto-ordenació.

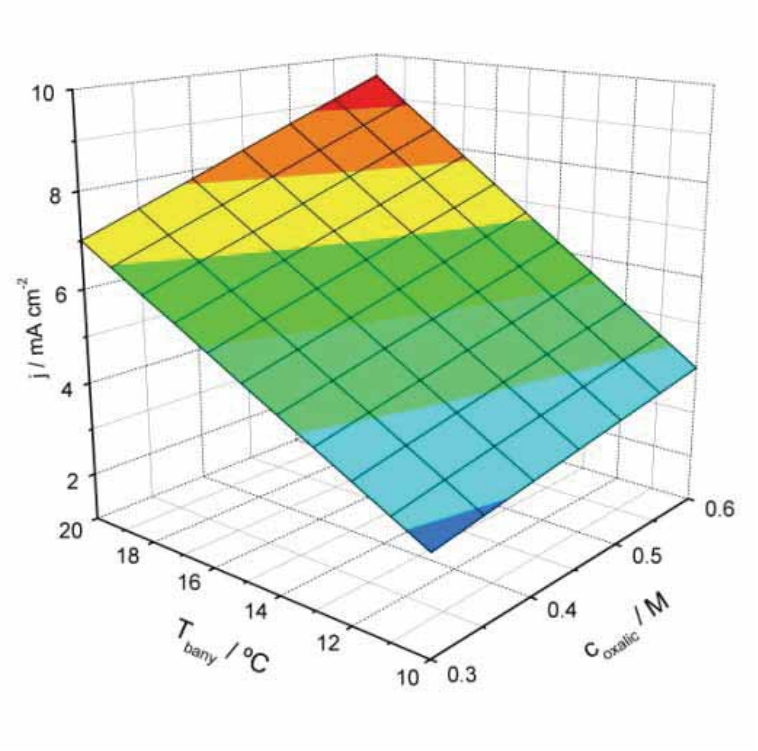

Figura 3.1. Dependència de la densitat de corrent amb la temperatura i la concentració del bany per a un procés d'anoditzat auto-ordenat en control de voltatge (45 V)

3.3.2. Anàlisi dels paràmetres estructurals de l'alúmina

Pel que fa als paràmetres estructurals de l'alúmina (d_{int} i $\delta_{cel\cdot la}$), s'ha comprovat que únicament estan determinats pel valor del voltatge que s'estableix a la interfase de l'alumini en ambdós modes de treball, fet conegut en un procés en control de voltatge [128, 132, 144, 165], però poc estudiat en un procés en control de corrent [190].

Els dos paràmetres (d_{int} i $\delta_{cel\cdot la}$) estan lligats geomètricament segons les expressions [3.f] o [3.g], en funció del model d'empaquetament hexagonal considerat (empaquetament de cel·les esfèriques o de cel·les hexagonals, respectivament).

[3.f] Cel·la esfèrica $$\delta_{cel\cdot la}(\mu m^{-2}) = \frac{4\cdot 10^6}{\pi\cdot[d_{int}(nm)]^2}$$

[3.g] Cel·la hexagonal $$\delta_{cel\cdot la}(\mu m^{-2}) = \frac{2\cdot 10^6}{\sqrt{3}\cdot[d_{int}(nm)]^2}$$

La $\delta_{cel\cdot la}$ s'ha determinat experimentalment comptant el número de porus en un fragment de superfície d'àrea coneguda d'una imatge de SEM. A partir d'aquest valor s'ha estimat un valor promig estadístic de la distància entre porus, segons les expressions anteriors. Les dades obtingudes s'han mostrat útils a l'hora d'extreure resultats i són coherents amb els valors establerts a la bibliografia.

En un procés en control de voltatge s'ha trobat que d_{int} no varia amb el temps, sempre que el voltatge no es modifiqui externament i, almenys, per a anoditzats de fins a tres hores (els més llargs assajats, amb gruixos de fins a 30 μm). També s'ha observat que la variació de d_{int} amb el voltatge aplicat coincideix amb l'establert a la bibliografia [132, 144, 158, 191]. La dependència és força lineal en un ampli rang de voltatges (35 V – 55 V), amb un pendent constant aproximadament de 2.6 nm·V^{-1} (±0.2). És a dir, el fet d'utilitzar un alumini menys pur no modifica el comportament esperat segons els estudis realitzats amb alumini > 99.999 %. En un procés en control de corrent, la dependència no és tan senzilla. Si s'analitza l'evolució temporal del voltatge, es troba que el paràmetre d_{int} presenta el mateix comportament que el descrit anteriorment, sempre que l'anoditzat finalitzi dins el interval de pseudo-estacionarietat (< 60 min). Per a anoditzats més llargs es detecta un augment continu del voltatge amb el temps a partir d'un cert moment, tal i com es descriu a [123]. S'han registrat augments de voltatge del 20 – 30 % en passar de 60 a 180 min. La peculiaritat del procés rau en el fet que la distància entre porus mesurada a la base de la capa porosa augmenta en concordança amb aquesta pujada del voltatge enregistrat. S'ha determinat que l'augment de d_{int} segueix el valor donat per la relació d_{int} - voltatge per als processos en control de voltatge (2.6 nm·V^{-1}). Aquest fet suggereix l'existència d'una interrelació entre el gruix de la capa porosa (que causa el increment de voltatge enregistrat amb el temps) i el camp elèctric establert a la capa barrera (que causa l'augment de d_{int} a la base dels porus). El problema de la difusió a través del porus, que en un procés en control de voltatge es revela en la disminució del corrent amb el temps (el camp elèctric és manté fix a la base dels porus), en un procés en control de corrent es manifesta en un augment del voltatge total enregistrat. Aquest fet produeix, en conseqüència, canvis progressius en l'estructura de la capa i constata una relació existent entre el camp elèctric generat a la capa barrera i el caràcter fisicoquímic de la interfase òxid – dissolució a la base del porus.

3.3.3. El fenomen de l'auto-ordenació en els dos modes de treball

D'altra banda s'ha trobat que el fenomen de l'auto-ordenació depèn exclusivament del voltatge, ja sigui aplicat (en un procés en control de corrent) o mesurat (en un procés en control de voltatge). En àcid oxàlic el fenomen de l'auto-ordenació es manifesta a voltatges entre 40 i 60 V en l'alumini utilitzat, tot i que s'ha escollit el valor de 45 V com a l'òptim per a la fabricació de capes auto-ordenades (a la bibliografia el valor més estès és de 40 V). A voltatges inferiors o superiors a aquest

rang l'estructura hexagonal auto-ordenada organitzada en dominis desapareix i es formen cel·les de geometria irregular,tant en control de voltatge com de corrent. En control de voltatge, les condicions experimentals semblen no afectar el comportament d'aquest fenomen, almenys en el rang assajat. En l'anoditzat en control de corrent, la resposta electroquímica del sistema varia amb les condicions experimentals aplicades. En aquest cas, es poden trobar diferents condicions experimentals que portin a l'auto-ordenació.

Altrament, s'ha observat un increment del desordre quan s'augmenta el temps d'anoditzat. La informació disponible sobre el procés d'auto-ordenació en un alumini d'elevada puresa (99.999 %) contradiu aquestes observacions [155, 156, 163]. En aquest cas, a majors voltatges o temps més llargs s'obté una millora de l'ordre. Aquests paràmetres d'operació no van en detriment de l'ordre, com en el nostre cas. La justificació rau en el fet d'utilitzar un alumini de baixa puresa. L'alumini, concretament, conté una sèrie de partícules intermetàl·liques inserides a la matriu (Al-Fe, Al-Si-Fe,...), de comportament electroquímic diferent respecte la matriu [185, 186, 192]. A mesura que avança el procés d'anoditzat, les partícules s'incorporen a la capa d'alúmina i causen una desestructuració local ja que la velocitat de creixement de l'anoditzat al seu interior és menor. Com més ràpid (majors densitats de corrent) o més llarg es realitza el procés, més gran és el número de partícules incorporades a la capa i pitjor l'ordenació obtinguda, arribant inclòs a desaparèixer completament. La figura 3.2a i 3.2b mostra el mecanisme de desestructuració que causa una partícula intermetàl·lica quan s'incorpora a la capa anòdica. S'ha comprovat que aquest efecte es propaga inclòs en el segon procés d'anoditzat, tal i com es mostra a la figura 3.2c.

3.3.4. La nanotexturació: capacitat d'adaptació en el doble anoditzat

En relació al procés d'anoditzat, finalment, també s'ha analitzat el fenomen de la nanotexturació de l'alumini en el procés del doble anoditzat i la importància en l'etapa de nucleació dels porus. És conegut que la creació d'un patró sobre la superfície de l'alumini serveix de punt de nucleació dels porus en un segon procés d'anoditzat [131, 152, 177, 178]. En aquest punt del treball, s'han creat una sèrie de nanotextures amb diversos valors de d_{int} (100 – 160 nm), mitjançant un primer anoditzat en control de voltatge amb diferents voltatges (35 – 55 V) segons l'expressió [3.h].

[3.h] $$d_{int}(nm) = 2.65 \cdot V(V) + 9.75$$

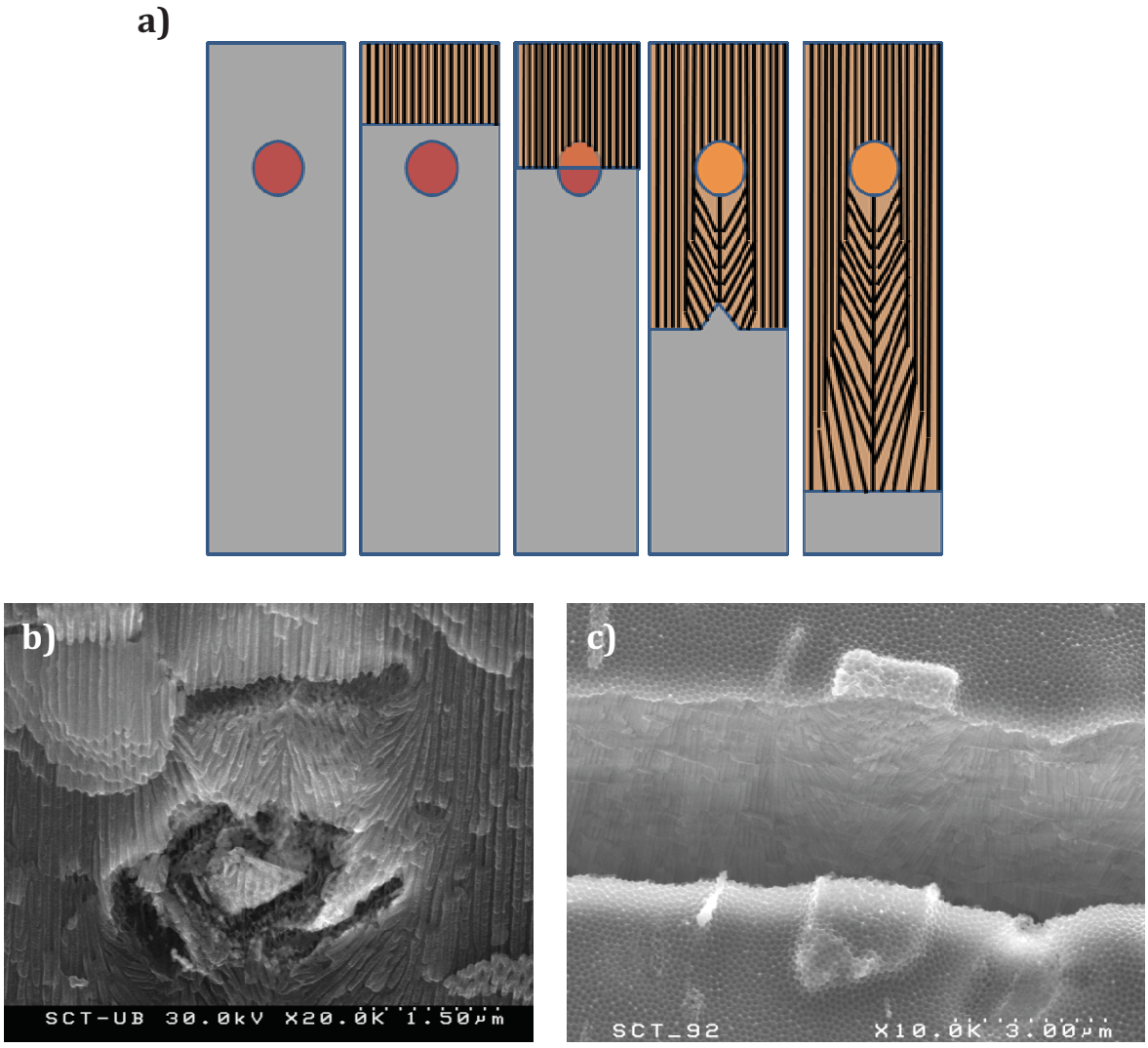

Figura 3.2. a) mecanisme d'incorporació de partícules intermetàl·liques durant l'anoditzat i desestructuració; b) partícula intermetàl·lica incorporada (en secció); c) partícula intermetàl·lica sobre la superfície d'alúmina anòdica (seccionada).

Les nanotextures creades s'han fet servir per créixer una segona capa d'alúmina anòdica, assajant-ne diferents voltatges (entre 35 i 55 V). S'ha analitzat la compatibilitat entre el procés de nucleació dels porus i els patrons marcats per la nanotextura i s'ha establert que, si el voltatge aplicat en el segon anoditzat és superior o igual al de la primera etapa ($V_{2AN} \geq V_{1AN}$), la nucleació dels porus procedeix segons el marcatge de la superfície, tal i com es mostra a l'article (pàg. 65). De tota manera, les últimes observacions han mostrat que el creixement de la capa segons aquesta nanotextura es conserva només durant un cert temps i que, com més gran és la diferència entre els voltatges aplicats, menys temps pot el sistema mantenir aquest patró. Les figures 3.3a i 3.3b mostren imatges SEM de seccions de capes d'alúmina anòdica, on s'observa com es produeix una disminució del número de porus quan la diferència de voltatges és gran (20 V en figura 3.3b) però no quan és petita (10 V en figura 3.3a), en aquest cas almenys per a les 5 µm primeres.

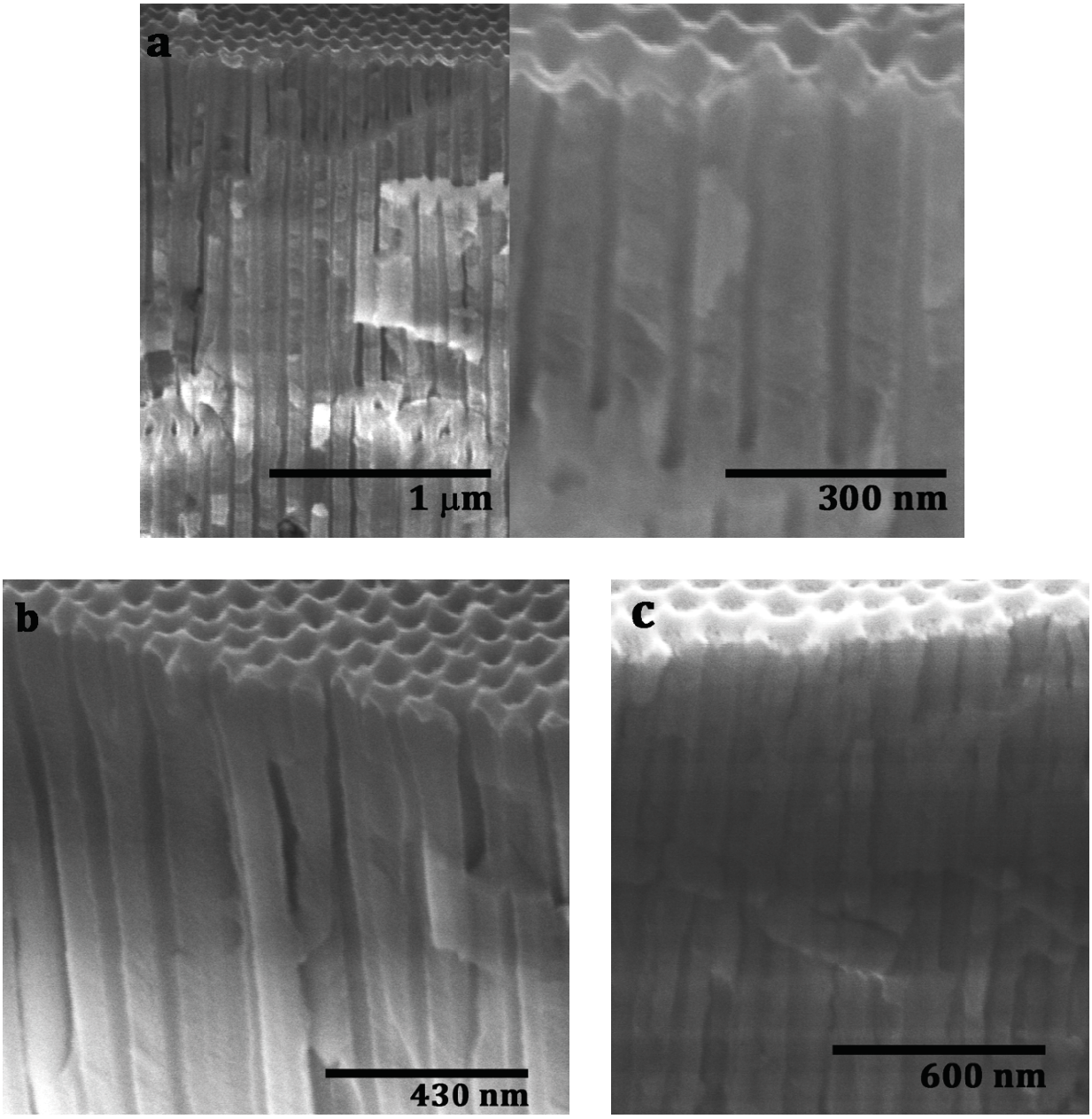

Figura 3.3. Imatges de SEM de seccions d'alúmina anòdica després de doble anoditzat potenciostàtic asimètric: a) V_{1AN} = 35 V, V_{2AN} = 45 V; b) V_{1AN} = 35 V, V_{2AN} = 55 V; c) V_{1AN} = 55 V, V_{2AN} = 35 V.

D'altra banda, si el voltatge aplicat en el primer anoditzat és superior al voltatge aplicat en el segon ($V_{1AN} > V_{2AN}$, figura 3.3c i article pàg.65), la nucleació dels porus procedeix sense influència de la nanotextura prèvia, produint-se la porositat corresponent al voltatge aplicat. En aquest cas es pot observar la nucleació de més d'un porus per unitat cel·lular de l'estructura, quantitat que depèn de la diferència de voltatge aplicada entre les dues etapes.

Aquest estudi s'ha revelat força útil a l'hora d'entendre les limitacions de la nanotexturació de l'alumini. Els resultats s'han aplicat amb èxit en el capítol 5, on s'ha emprat una superfície d'alumini nanoimpresa per a la generació de membranes

d'alúmina amb un monodomini hexagonal perfecte i on la correcta nucleació dels porus als emplaçaments prefixats depèn en gran mesura de l'optimització dels paràmetres del procés per a cada nanotextura utilitzada.

3.4. Propietats tèrmiques de l'alúmina anòdica: estudi de la viabilitat en l'aplicació en dispositius sensors de gasos

Per a concloure aquest capítol, es presenten els resultats obtinguts en l'estudi del comportament de l'estructura d'alúmina porosa al sotmetre-la a diferents tractaments tèrmics de recuit. L'objectiu és analitzar la viabilitat de les membranes d'alúmina anòdica, després d'eliminar el substrat d'alumini, com a possibles plataformes suport per a la fabricació de sensors de gasos. Aquests dispositius requereixen un material que sigui resistent als xocs tèrmics, sense que pateixi canvis estructurals importants, ja que han de ser sotmesos a un número elevat de cicles de temperatura elevada (> 900 ºC) per permetre la detecció del gas en qüestió. Es proposa la utilització de membranes d'alúmina porosa com a alternativa al silici (el material base més utilitzat en microelectrònica), ja que presenta un alt punt de fusió (2054 ºC respecte els 1410 ºC del silici) i una baixa conductivitat tèrmica (alúmina a 20 ºC: 30 $W \cdot m^{-1} \cdot K^{-1}$, silici a 20 ºC: 4980 $W \cdot m^{-1} \cdot K^{-1}$), que s'accentua per la seva porositat (~ 13 % en àcid oxàlic a 45 V, 0.30 M i 20 ºC). D'aquesta manera es podria escalfar el sensor molt localment a través d'una resistència elèctrica dibuixada per serigrafia i així evitar la degradació dels altres components del dispositiu.

En principi, l'estudi mostra que l'alúmina anòdica presenta unes propietats mecàniques adequades per a aquesta aplicació, inclús després de tractaments tèrmics extrems. De tota manera, la capa barrera s'ha revelat fonamental en l'estabilitat tèrmica de la membrana. A pesar de tenir un gruix d'unes poques desenes de nanòmetres (la capa barrera és aproximadament 240 vegades més prima que la capa porosa en les condicions de preparació), li confereix estabilitat mecànica capaç de contrarestar els efectes de dilatació tèrmica durant els cicles tèrmics. En cas d'eliminar aquesta capa, els fenòmens de dilatació i les transformacions de fase estressen l'estructura porosa, que s'enguerxeix o es fractura. Una membrana tractada a 1100 ºC sota una càrrega pot suportar a continuació diversos cicles tèrmics a temperatures iguals o inferiors. No s'observa cap altre canvi, demostrant-ne l'estabilitat mecànica als processos tèrmics i la viabilitat de la seva implementació en aquest tipus de dispositius.

També s'han estudiat les transformacions cristal·logràfiques que es produeixen en l'alúmina anòdica després d'un tractament de recuit a diferents temperatures i s'han observat els següents fets:

- La membrana d'alúmina anòdica presenta d'origen una estructura cristal·lina amorfa, que incorpora aigua i ions del bany. Durant el tractament a temperatures inferiors a 750 ºC, la membrana es deshidrata i es mineralitza el contingut iònic, que és de naturalesa orgànica (procedent dels anions oxalat del bany). No hi ha cap altre canvi cristal·logràfic en l'estructura.

- A partir de 900 ºC s'observa la formació de les fases γ-Al_2O_3 i α-Al_2O_3. Aquesta última fase s'ha pogut assignar integrament a la cristal·lització de la capa barrera, i no la de la capa porosa, la qual és la responsable de l'estabilitat mecànica als processos tèrmics de la membrana. S'ha determinat que el gra, segons la fórmula de *Scherrer* [3.i], és més fi en la fase γ que en la α. Aquest fet s'ha associat a la alta compacitat i puresa de la capa barrera, en la qual els grans poden desenvolupar-se amb més facilitat, respecte la porositat i grau d'impura de la capa porosa, el que dificulta el creixement dels grans.

[3.i] $$D = \frac{K \cdot \lambda}{\beta \cdot \cos\theta}$$

- Els tractaments tèrmics afecten la morfologia de la membrana, però sense destruir-la. Es manté l'estructura porosa, però es produeix un canvi progressiu. La cristal·lització de la capa porosa transforma la superfície *on-top* de la morfologia típica del primer anoditzat a la morfologia esperada per a un segon anoditzat, però sense ordenació. La capa barrera no sofreix cap canvi morfològic destacable durant la cristal·lització.

Recull d'articles englobats en el capítol 3

Pàg. 57: Influence of the aluminum surface on the final results of a two-step anodizing
J.M. Montero-Moreno, M. Sarret, C. Müller, Surface and Coatings Technology 201 (2007) 6352

Pàg. 65: Some considerations on the influence of voltage in potentiostatic two-step anodizing of AA1050
J.M. Montero-Moreno, M. Sarret, C. Müller, Journal of The Electrochemical Society 154 (2007) C169

Pàg. 73: Setting a self-ordered alumina template by two-step galvanostatic anodizing: nanotexturing and mechanism notions
J.M. Montero-Moreno, M. Sarret, C.M. Müller, enviat a Electrochimica Acta el 5 de Març de 2009

Pàg. 81: Assessment of the thermal stability of anodic alumina membranes at high temperatures
L. Fernández-Romero, J.M. Montero-Moreno, E. Pellicer, F. Peiró, A. Cornet, J.R. Morante, M. Sarret, C. Müller, Materials Chemistry and Physics 111 (2008) 542

Influence of the aluminum surface on the final results of a two-step anodizing

Available online at www.sciencedirect.com
ScienceDirect
Surface & Coatings Technology 201 (2007) 6352–6357
SURFACE & COATINGS TECHNOLOGY
www.elsevier.com/locate/surfcoat

Influence of the aluminum surface on the final results of a two-step anodizing

J.M. Montero-Moreno, M. Sarret, C. Müller *

ELECTRODEP, Department of Physical Chemistry, University of Barcelona, Martí i Franquès 1, 08028-Barcelona, Spain

Received 18 October 2006; accepted in revised form 4 December 2006
Available online 31 January 2007

Abstract

1050 Aluminum alloy sheets were used to analyze the influence of a surface treatment on the characteristics of the alumina layer formed in a two-step anodizing. The study was mainly focused on two pretreatment steps, electropolishing and acid etching, as well as on the intermediate stripping step. The pretreatment procedure was optimized by accounting for the chemical nature of the substrate, with the results indicating that additional pretreatment steps enhanced the self-ordered porous arrangement. The *E–t* curves recorded during the experiments demonstrated that the best alumina layers were obtained when the first barrier layer had a high resistance; i.e., a high anodizing potential. The application time of the stripping step was optimized to clean the surface from alumina remains, without damaging the aluminum substrate. By optimizing all of these experimental conditions, we were able to obtain porous anodic aluminum oxide layers displaying ordered domains several hundreds of nanometers in length.

Keywords: AA1050; Two-step anodizing; Electropolishing; Stripping

1. Introduction

Anodic aluminum oxide (AAO) is a self-ordered material suitable as a template for obtaining nanostructured materials. Although these materials were initially used in magnetic and/or electronic devices, their applications fields are steadily increasing [1–4]. In recent years, most research has been focused on obtaining AAO templates with a cellular structure as ordered as possible, which is achieved by minimizing the formation of defects across the entire layer. To this end, different methods have been developed: nano-indentation of the aluminum surface [5]; focused ion beam techniques [6]; and the two-step anodizing procedure [7]. The common aim of these procedures is to imprint the aluminum surface with a regular pattern, since this pattern will act as a seed for the growth of alumina pores.

Whatever experimental approach employed, the state of the aluminum surface is a key factor in obtaining self-ordered AAO layers [8–10]. This means that the surface pretreatment must be carefully selected, particularly when an aluminum alloy is used. Different steps must be performed to clean the natural surface oxides and to reduce the number of intermetallic compounds present on the surface. Moreover, to reduce the surface roughness, additional steps must be included, such as chemical or mechanical polishing and electropolishing. The surface roughness is an important parameter to take into account when AAO layers of high quality must be obtained.

For this study, a standard two-step anodizing procedure was applied to obtain porous AAO layers as regular and homogeneous as possible. As a first attempt, we selected a 1050 aluminum alloy for our study in order to check the effect of intermetallic particles on the application of this anodizing technique. This alloy was chosen taking into account that, among aluminum alloys, 1050 boasts the highest Al content (99.5% Al minimum). However, the small amount of alloying elements is sufficient to modify the pretreatment process, because some new steps must be included to remove these intermetallic particles from the surface. In this context, the present study carried a double objective: to determine the influence of both the pretreatment and stripping procedures on the characteristics of the final alumina layers. Taking into account that the usefulness of electropolishing and acid etching pretreatment steps remains questionable, special attention was paid to the influence these steps exerted on the overall process.

* Corresponding author.
E-mail address: c.muller@ub.edu (C. Müller).

0257-8972/$ - see front matter © 2006 Elsevier B.V. All rights reserved.
doi:10.1016/j.surfcoat.2006.12.003

2. Experimental procedures

Commercial sheets of AA1050 (27 mm × 27 mm × 0.7 mm) were used. The alloy consisted of relatively pure aluminum (99.5%) with Fe (<0.30%) and Si (<0.20%) as the principal alloying elements.

Pretreatment of the aluminum surface prior to anodizing involved five steps. The initial steps were based on an industrial procedure, which took into account the composition of the AA1050 substrate: 1) alkaline degreasing (AKD) in METEX T5-40A® at 55 °C; 2) alkaline etching (AKE) in a NaOH: Gluconate 5:3 (w:w) solution at 55 °C; 3) desmutting (DM) in HNO_3 30% at room temperature. Finally, to reduce the roughness of the surface, two additional self-scaled steps were applied: 4) galvanostatic electropolishing (EP) in H_3PO_4:H_2SO_4 solution 3:2 (at 15 Adm^{-2}). The temperature was optimized as a function of porous AAO structure, monitored by the *E–t* anodic response; 5) acid etching (ACE) in H_3PO_4:CrO_3 3.5%:2% at 55 °C. Composition and time were analyzed to obtain an accurate dissolution of the oxide formed during electropolishing.

Samples were strongly rinsed in double-distilled water after each step. All solutions were prepared with analytical grade reagents and double-distilled water.

A two-step galvanostatic (1 Adm^{-2}) anodizing process in a 0.60 M oxalic acid electrolyte at 20 ± 0.2 °C was applied. In this process, immediately after the surface pretreatment, aluminum sheets were anodized for 1 h in the oxalic acid bath (referred to as 1AN). Then, the AAO layer was stripped in an H_3PO_4:CrO_3 3.5%:2% solution at 55 °C (referred to as ST) and a second anodizing step (referred to as 2AN) was immediately carried out for 1 h. Finally, samples were strongly rinsed in double-distilled water, air dried, and stored in a vacuum.

A thermostatized two-electrode cell (2 L) was employed with a cylindrical lead cathode and agitation by air. The temperature was regulated with a Polyscience cryostat (model 9106) while a power supply from GRELCO Inc. (model GE2501DVG) was used to apply current (max. 1 A) to the cell. The control of the system response was monitored with a HP34401A multimeter. Data were transferred to a PC.

Monitoring of the aluminum surface during different stages of the anodizing process was carried out using a white light interferometer from Zygo Corporation and an AFM with a Multimode from Digital Instruments-Veeco.

FE-SEM (HITACHI S-4100FE) was used to analyze the morphology of the AAO layers to include both on-top (outer surface of AAO) and on-bottom (inner surface of AAO) viewings. On-bottom preparation of the samples consisted of four steps. Samples were anodized on both sides. First, the side of interest was protected with a lacquer while the reverse side was etched in a concentrated NaOH solution to expose the underlying aluminum. The alloy was then dissolved in a $CuCl_2$: HCl (1.2%):(20%) aqueous solution. An optional variation involved etching the barrier layer in the alumina membrane with a H_3PO_4 5% solution, the amount of time dependent upon its thickness.

The thickness of the alumina film was measured by the Eddy current method (DUALSCOPE - FISCHER Inst.). Brightness was determined using a micro-gloss from BYK-Gardner with an angle of incidence of 60°.

3. Results and discussion

Anodizing of the AA1050 samples was performed in oxalic acid baths at fixed conditions to analyze only the influence of the pretreatment and stripping procedures. As the aim of the study was to obtain a regular and ordered alumina structure, the effectiveness of these steps was assessed by analyzing the alumina layer morphology at different levels.

3.1. Influence of aluminum surface pretreatment

The effects of the different pretreatment steps on the 1050 aluminum alloy surface was monitored using interferometric and AFM images. Fig. 1 shows the interferometric images of the aluminum surface, including the rms values obtained after the initial steps (AKD, AKE and DM). The aim of these steps was to obtain a clean surface and to diminish the amount of intermetallic compounds on the surface. As mentioned above, we accounted for the composition of the aluminum substrate, maintaining the requisite conditions throughout the study. As

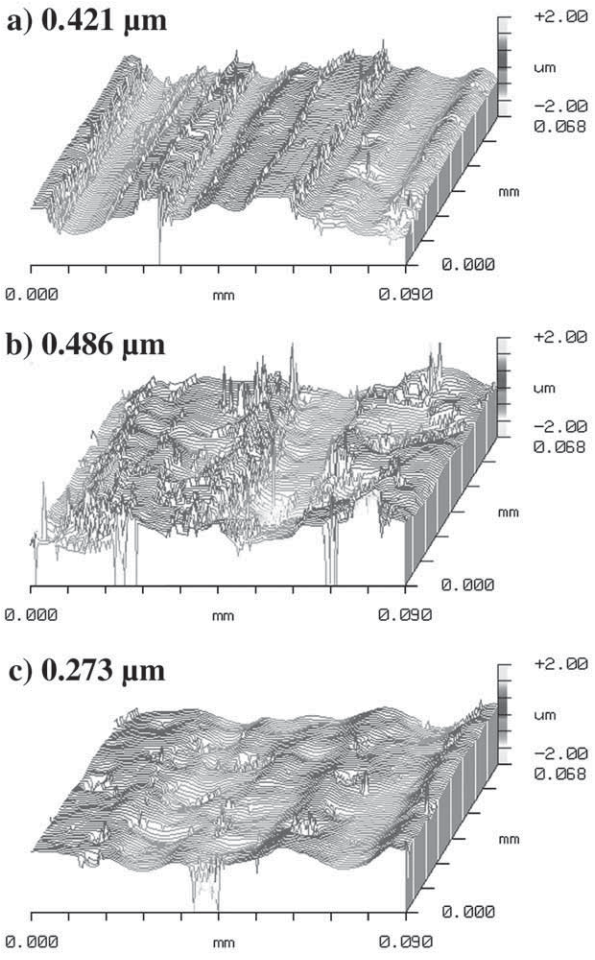

Fig. 1. Interferometric images (×40) of the aluminum surface after a) AKD; b) AKE; c) DM. Measured rms is included.

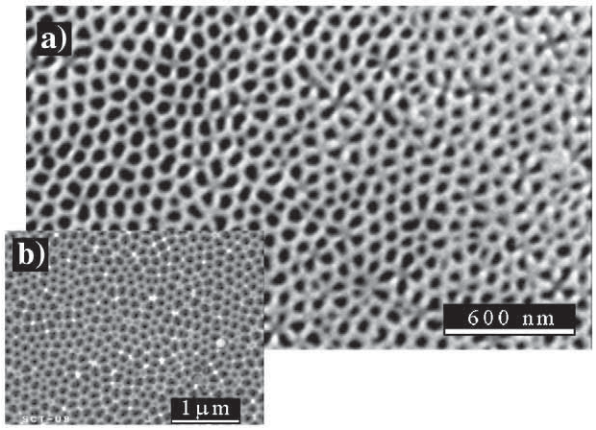

Fig. 2. SEM images of the AAO surface obtained with AKD+AKE+DM pretreatment. a) On-bottom view after single-step anodizing and b) on-top view after two-step anodizing. Anodizing conditions: t_{anod}=1 h; j_{anod}=1 Adm^{-2}; oxalic acid 0.60 M; T=20 °C.

can be seen in Fig. 1, the morphology of the aluminum surface changed, although these alterations were not always reflected by the roughness values. During the AKE, the formation of precipitates (smut) altered the surface appearance without any apparent change in the rms value. At the DM step, these precipitates were dissolved and a clear decrease in the rms value was observed.

Fig. 2a shows the on-bottom micrograph of the alumina layer obtained after a 1 h single-step anodizing, with pretreatment consisting only of the aforementioned steps. Although a well-defined porous structure was observed in the image, no domains were identified. This disordered structure remained unchanged when a two-step anodizing was performed using the same pretreatment conditions (Fig. 2b).

Thus, employing a simple pretreatment procedure with AA1050 yielded surfaces too rough to obtain ordered alumina layers, even with a second anodizing step. To improve the order of the alumina layers, the samples were electropolished and acid etched following the DM step. Fig. 3 shows the interferometric images of the aluminum surface after both processes. With proper electropolishing, rms decreased significantly and the aluminum samples appeared specular, albeit with a soft whitish tonality. When the sheets were acid etched, the roughness was similar but the surface appeared totally specular.

Since the latter technique did not clearly explain the ACE effect, the samples were examined using AFM (Fig. 4). At this scale, the surfaces proved very different in both appearance and "nano" roughness. After the EP step, some oxide precipitates and/or intermetallic particles remained on the surface and were responsible for its whitish appearance. The aim of the final ACE step was to minimize the amount of these surface defects and to obtain the smooth surface shown in Fig. 4b); i.e. a mirror-like finished appearance. The influence of the EP and ACE steps on the final morphology of alumina layers can be inferred by comparing Figs. 2 and 5: with the complete pretreatment, the

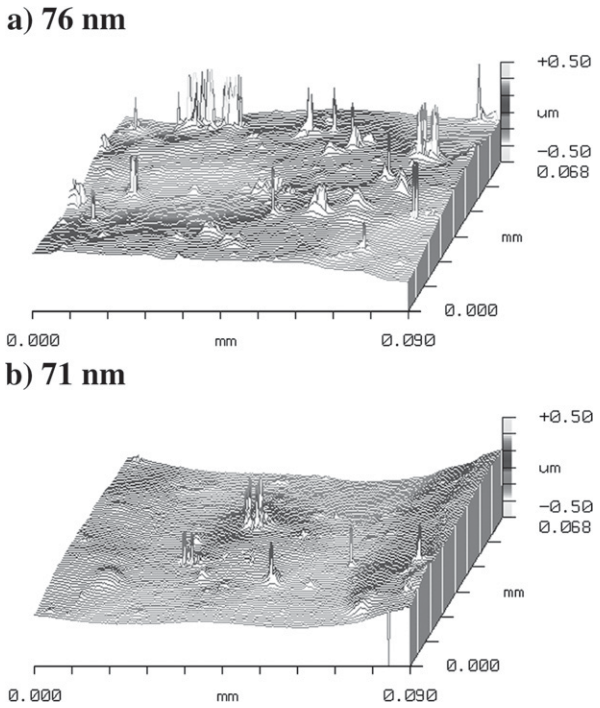

Fig. 3. Interferometric images (×40) and measured rms of the aluminum surface after a) EP; b) ACE in H_3PO_4:CrO_3.

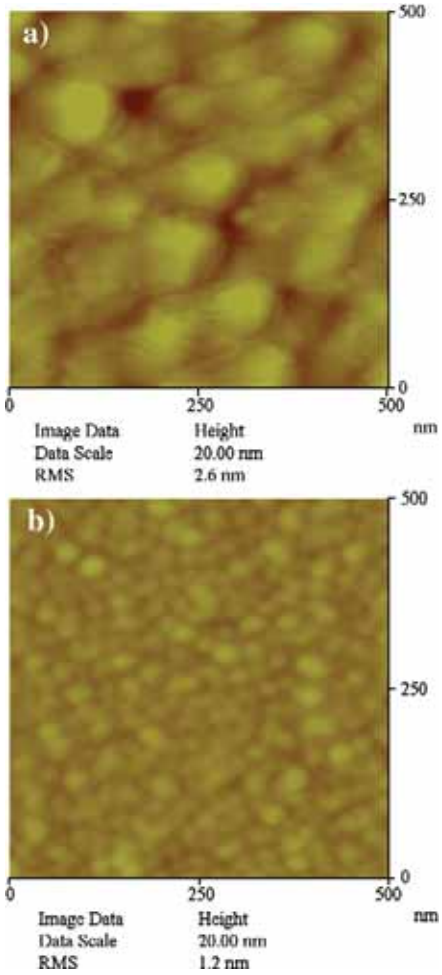

Fig. 4. AFM images of the aluminum surface after a) EP (rms=2.6 nm); b) ACE in H_3PO_4:CrO_3 (rms=1.2 nm).

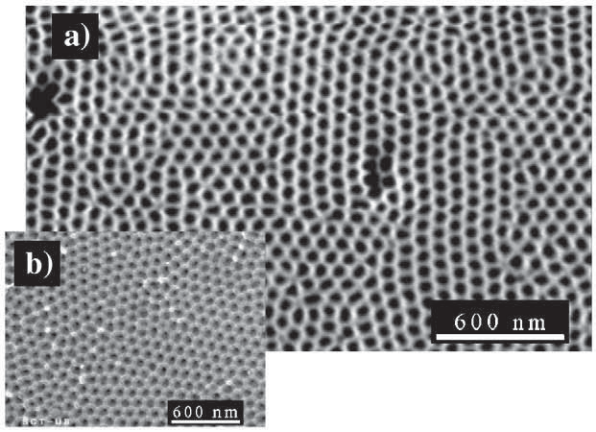

Fig. 5. SEM images of the AAO surface with EP and ACE pretreatments a) on-bottom view after single-step anodizing b) on-top view after two-step anodizing. Anodizing conditions: t_{anod}=1 h; j_{anod}=1 Adm^{-2}; oxalic acid 0.60 M; T=20 °C.

porous structure showed enhanced order and homogeneity, both after the first (Fig. 5a) and second anodizing (Fig. 5b). In contrast to Fig. 2, domains measuring several hundreds of nanometers were clearly visible in these samples.

However, to obtain these ordered alumina layers the working conditions for these two final pretreatment steps had to be accurately controlled. Once the electrolyte and electrochemical conditions were selected, the electropolishing temperature had to be checked, since it affected the viscosity of the anodic film formed during this process and modified the applied voltage. The *E–t* curves recorded during the EP and 1AN processes were useful in explaining the influence of this parameter (Fig. 6). The curves clearly demonstrated that the EP conditions affected the first steps of the anodizing process: the initial potential increase, which resulted from the formation of the high resistance barrier layer, and the potential maximum, which was related to the breakdown of the layer from nucleation and growth of pores [11]. However, the final stationary conditions of the AAO growth were not dependent upon the pretreatment conditions.

At the lowest temperatures (55–65 °C), the electropolishing voltages were the highest (Fig. 6a) while the anodizing voltage peaks were the lowest (Fig. 6b). If the temperature was too low, the viscosity of the film increased and a compact insoluble oxide layer tended to form (the whitish oxide layer), which increased the ohmic drop and promoted a voltage increase. By increasing the temperature, this oxide tended to disappear with the electropolishing voltage decreasing. Under these conditions, the anodizing voltage peak increased because a more compact barrier alumina layer was formed during anodizing. Above 80 °C, however, the electropolishing voltage proved lower than expected and the anodizing voltage peak decreased. At very high temperatures, viscosity decreased and the poor ohmic drop differentiation between the surface peaks and valleys involved a very low applied potential. Under these conditions, no effective electropolishing occurred, roughness increased, and the effects of the final acid etching were useless.

The samples obtained in these experiments were observed by AFM and our results matched those suggested by the *E–t* curves: i.e., the best electropolishing temperature for a smooth, specular aluminum surface was 77.5 °C, at which the maximum anodizing peak voltage was observed. Under these conditions, the resulting porous alumina structure following anodizing possessed the optimum morphology for future applications. This fact suggested that in order to obtain a regular and homogeneous porous AAO layer during anodizing, the development of the barrier layer was essential. If a non-compact barrier layer formed during the initial seconds of anodizing, the peak intensity remained low and a poorly ordered pore distribution resulted. Conversely, if a compact oxide was formed, layer breakdown was more uniform and homogeneous while peak intensity increased, resulting in a more ordered pore nucleation across the surface.

In conclusion, following the EP plus ACE processes, AA1050 samples with a fine-grained surface and a very low rms were obtained. Examining the samples after the first and second anodizing, we determined that inclusion of these processes enhanced self-ordered porous arrangements.

3.2. Two-step anodizing: optimization of the stripping step

It is known that two-step anodizing can improve the structure of the porous AAO layer [12–15]. With this process, the aluminum alloy sheets are anodized twice, although the intermediate forming alumina layer must be stripped. The aim of the stripping process is to prepare the aluminum surface for a

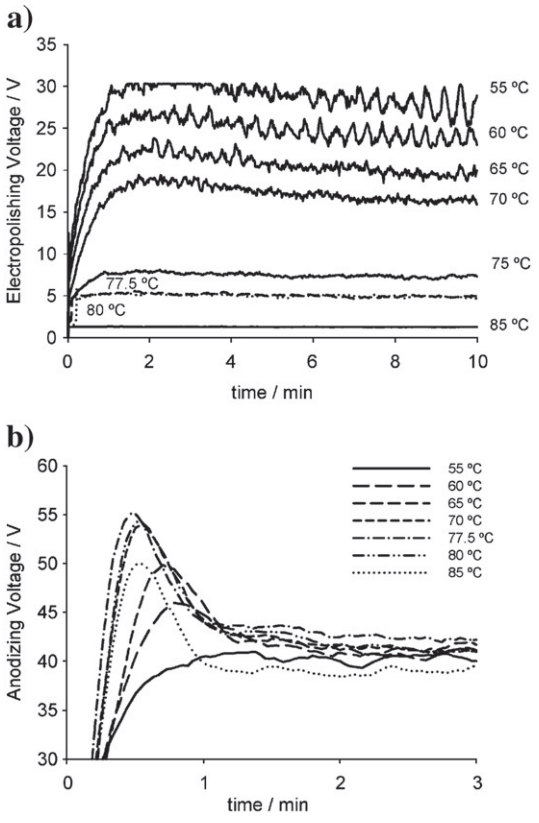

Fig. 6. *E–t* curves for a) EP at 15 Adm^{-2} in H_3PO_4:H_2SO_4 3:2 and b) 1AN step: 1 h at 1 Adm^{-2} in oxalic acid 0.60 M and 20 °C, at different electropolishing temperatures.

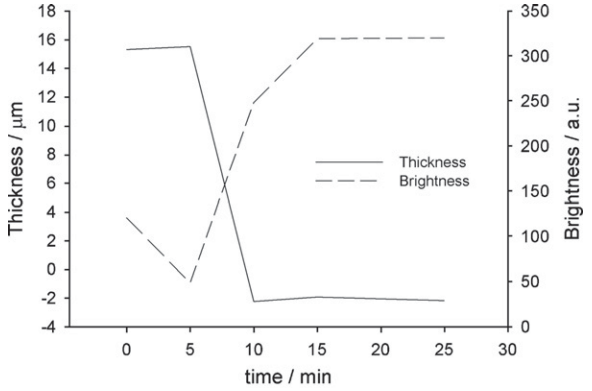

Fig. 7. Evolution of thickness and brightness over time during the stripping of the first alumina layer. 1AN step conditions: t_{anod}=1 h; j_{anod}=1 Adm^{-2}; oxalic acid 0.60 M; T=20 °C.

new anodic oxidation. The composition of the solution, the bath temperature and the application time must be accurately defined to obtain a very smooth surface. In this step only the AAO layer must be etched, without modifying the aluminum surface.

The solution used in this study was a common mixture of a CrO_3 and H_3PO_4 and the application time was controlled to optimize the process. If the application time becomes prolonged, then aluminum surface is damaged. If the application time is too short, structured alumina remains on the surface. Obviously, the temperature of the stripping bath highly influences the rate of this process. Although it might prove interesting to employ a high temperature, one must remember that the process cannot be implemented too quickly or the control time will be jeopardized. The temperature that best balanced stripping rate and time was 55 °C. In this second part of our study, pretreatment conditions prior to the first anodizing were identical to those described in the previous section.

To determine the time needed to obtain a clean surface, the thickness of the AAO layer and the surface brightness were used as control parameters. The graph in Fig. 7 shows the evolution of the layer thickness and the surface brightness during the stripping process. The thickness remained constant for a time and then decreased suddenly to 0, whereas brightness increased at the same time. These results can be explained by the stripping model schematized in Fig. 8. The alumina pores were initially filled with solution. Stripping then began over the inner pore alumina, ending on the pore walls. Thus, the diameter of pores initially increased without affecting the thickness of the layer (horizontal segment in Fig. 7). As the pore walls were dissolved, thickness decreased; when completely dissolved, the structure collapsed. At that particular moment, oxides rests remained across the surface (visible to the naked-eye) and it was impossible to measure the thickness. During the process, brightness increased as the surface changed from ceramic to metallic and extra time was needed to reach stationary values. By combining the brightness measurements with SEM observations, we established that the time (in min) needed for optimum stripping of the layer, without affecting the pattern on the aluminum surface, was twice the thickness of the alumina layer (in μm).

Fig. 9 shows the morphology of the alumina surface after the second anodizing step, when exposure time to the stripping solution was either too brief (Fig. 9a) or properly selected (Fig. 9b). For short times intervals rests belonging to the first anodizing layer were observed on the surface, which led to high roughness values. These rests were alumina nanowires that originated with the first anodizing layer and which corresponded

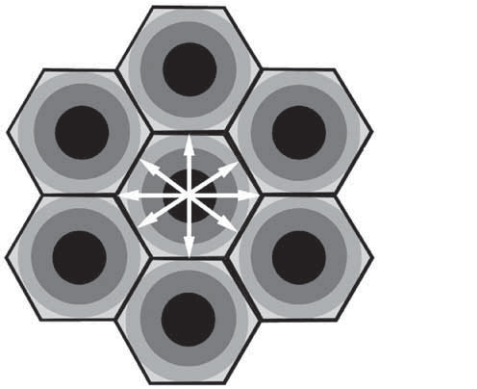

Fig. 8. Schematic diagram of the stripping process. Arrows shows the evolution of the dissolution of the alumina cell, which goes from the pore (the hydrated aluminum hydroxide — the darker gray circles) to the cell walls and vertices (the amorphous aluminum oxide — the lighter gray circles).

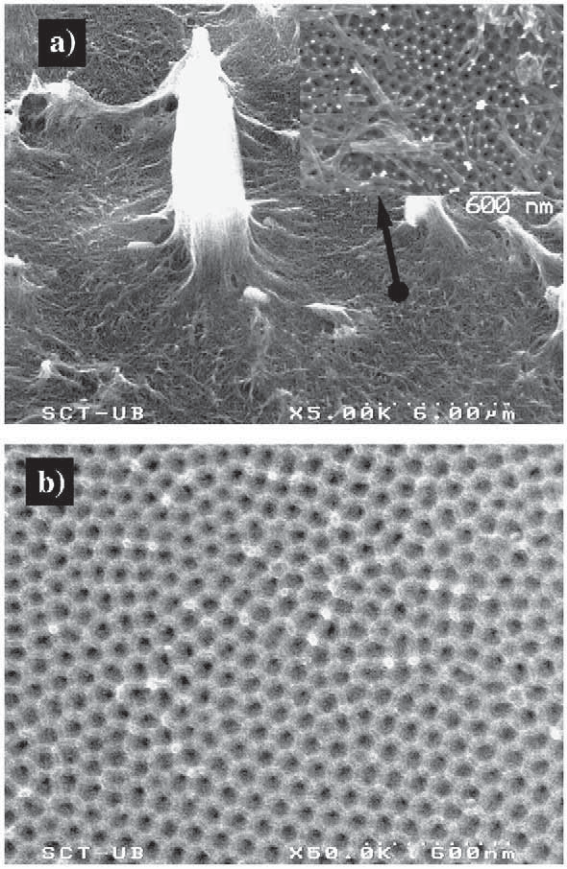

Fig. 9. SEM images of the alumina layer with a) an incorrect and b) correct stripping step after the second anodizing process. 1AN step conditions: t_{anod}=1 h; j_{anod}=1 Adm^{-2}; oxalic acid 0.60 M; T=20 °C.

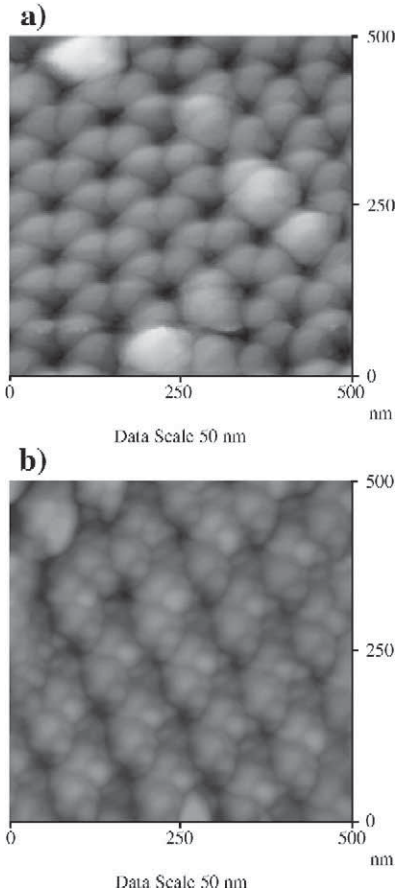

Fig. 10. AFM images of the aluminum surface after a) 1AN+ST and b) 2AN+ST. Anodizing conditions: t_{anod}=1 h; j_{anod}=1 Adm^{-2}; oxalic acid 0.60 M; T=20 °C.

to the vertices of the cells, the last area to be etched during the stripping process (Fig. 8).

Finally, the advantages of applying additional stripping+anodizing steps were analyzed. Results indicated that the ordering of the porous layer obtained from the second anodizing depended on those modifications of the aluminum surface promoted by the stripping. Fig. 10a shows the AFM image of the aluminum surface just before the second anodizing (after 1AN+ST). When this image was compared with that of Fig. 4b, which was obtained prior to the first anodizing (after pretreatment), we observed that the main difference was the occurrence of nanoimprinting on the aluminum surface after ST. This was responsible for the more ordered growth of the AAO layer in the 2AN process. Fig. 10b shows the AFM image of the aluminum surface after 2AN+ST. As a relatively small change was observed in the nanoimprinting structure of the aluminum, a third anodizing failed to significantly improve the porous layer structure: i.e., it was not worth applying additional anodizing steps for AA1050.

4. Conclusions

The pretreatment and stripping conditions needed to obtain ordered alumina layers after anodizing AA1050 samples were optimized. Our results demonstrated that the inclusion of electropolishing and acid etching during the pretreatment of this aluminum alloy improved the quality of the AAO layers, even when a two-step anodizing was applied. The electropolishing temperature affected the anodizing process to a high degree, since it modified the formation and breakdown of the barrier layer. The changes promoted by this pretreatment were analyzed by combining the *E–t* curves with SEM images. Our results indicated that the *E–t* curves were useful in controlling the effectiveness of the anodizing process. From these curves, we deduced that the best alumina layers were formed when the maximum anodizing potential reached its highest values: i.e., the initial barrier layer needed to have a high resistance, in such a way that its sudden breakdown promoted the homogeneous growth of porous over the aluminum surface.

In regards the stripping step, the appearance of the final alumina layer depended to a high degree on its correct application. For a given stripping solution, the requisite time had to be correctly balanced in order to achieve a completely clean surface without damaging the aluminum substrate. By combining of thickness and brightness measurements, we established that the stripping time (min) had to be twice the thickness (μm) of the alumina layer when employing the stripping solution used in this study.

Acknowledgments

The authors wish to thank the *Serveis Cientificotècnics (Universitat de Barcelona)* for the use of their equipment. This paper was supported by contract MAT 2003-09483 from the MEC. J.M. Montero would like to thank the DURSI for financial support.

References

[1] P.R. Evans, G. Yi, W. Schwarzacher, Appl. Phys. Lett. 76 (2000) 481.
[2] F. Li, R.M. Metzger, W.D. Doyle, IEEE Trans. Magn. 33 (1997) 3715.
[3] O.K. Varghese, D. Gong, M. Paulose, K.G. Ong, C.A. Grimes, E.C. Dickey, J. Mater. Res. 17 (2002) 1162.
[4] H. Asoh, M. Matsuo, M. Yoshihama, S. Ono, Appl. Phys. Lett. 83 (2003) 4408.
[5] H. Masuda, H. Yamada, M. Satoh, H. Asoh, Appl. Phys. Lett. 71 (1997) 2770.
[6] N.W. Liu, A. Datta, C.Y. Liu, L. Wang, Appl. Phys. Lett. 82 (2003) 1281.
[7] H. Masuda, K. Fukuda, Science 268 (1995) 1466.
[8] P. Bocchetta, C. Sunseri, R. Masi, S. Piazza, F. Di Quarto, Mater. Sci. Eng., C, Biomim. Mater., Sens. Syst. 23 (2003) 1021.
[9] M.T. Wu, I.C. Leu, M.H. Hon, J. Vac. Sci. Technol., B 20 (2002) 776.
[10] M.T. Wu, I.C. Leu, M.H. Hon, J. Vac. Sci. Technol., B 22 (2004) 2326.
[11] P.G. Sheasby, R. Pinner, The Surface Treatment and Finishing of Aluminum and its Alloys, Vol. 1, p. 11, 6th ed., Finishing Publications LTD. with ASM International, 2001.
[12] A.P. Li, F. Müller, A. Birner, K. Nielsch, U. Gösele, J. Vac. Sci. Technol., A, Vac. Surf. Films 17 (1999) 1428.
[13] A.P. Li, F. Müller, U. Gösele, Electrochem. Solid-State Lett. 3 (2000) 131.
[14] G.D. Sulka, S. Stroobants, V. Moshchalkov, G. Borghs, J.-P. Celis, J. Electrochem. Soc. 149 (2002) D97.
[15] G.D. Sulka, K.G. Parkola, Thin Solid Films 515 (2006) 338.

Some considerations on the influence of voltage in potentiostatic two-step anodizing of AA1050

Journal of The Electrochemical Society, **154** (3) C169-C174 (2007)
0013-4651/2007/154(3)/C169/6/$20.00 © The Electrochemical Society

Some Considerations on the Influence of Voltage in Potentiostatic Two-Step Anodizing of AA1050

J. M. Montero-Moreno, M. Sarret, and C. Müller*,z

ELECTRODEP, Department of Physical Chemistry, University of Barcelona, 08028 Barcelona, Spain

The two-step potentiostatic anodizing process of a 1050 aluminum alloy (AA1050) in an oxalic electrolyte was studied. Special attention was paid to the effect of the applied anodic voltage on the dimensions, homogeneity, and order of the anodic alumina porous layer obtained after a second step. The experimental conditions for obtaining homogeneous and ordered anodic aluminum oxide layers were defined. The effect of symmetric (the same applied voltage in the two anodizing steps) and asymmetric signals (different applied voltages in the first and second anodizing step) on the structure and geometry of the porous layer was studied. When the first anodizing voltage was higher than the second, the pore/cell ratio was greater than 1, meaning that the structure had more than one pore per cell.
 [DOI: 10.1149/1.2426880]

Manuscript submitted October 3, 2006; revised manuscript received October 26, 2006. Available electronically January 17, 2007.

Porous anodic aluminum oxide (AAO) films have attracted significant interest in recent years as they can be obtained conveniently and inexpensively and are extremely useful in nanoscience studies. The characteristic structure of AAOs is a hexagonal cell arrangement that grows perpendicular to the surface. This makes them suitable as templates for synthesizing new materials. Recently, self-ordered porous AAO have been extensively used to fabricate various nanostructures, such as nanoporous films, nanowires, or nanotubes, for a variety of promising applications.[1-4] The properties of these new materials are defined by the dimensions and morphology of the templates. Therefore, anodization has a great influence on the feasibility of fabricating these new nanostructures, due to the possibility to attain highly ordered porous AAO with the desired geometry. Nevertheless, accurately controlling these structures is a complex process, as many parameters have to be defined throughout the entire process.

AAO and its properties have been studied for many years. In fact, the interesting small-scale pore structure of the alumina was observed over 40 years ago.[5] It is widely accepted that the anodic structure is the result of coupled processes, which reach stationary conditions when aluminum is immersed in an electrolyte solution and electrochemical oxidation is performed. The first step is the formation of a barrier layer and the nucleation and growth of a porous layer over this compact alumina film. Subsequently, the system stabilizes and stationary conditions are attained due to two competitive processes: oxide formation at the metal/oxide interface and the chemical etching of the alumina at the bottom of the pores.

The formation mechanism of this complex structure is still under study. In addition to the basic initial papers on this field (see references included in Ref. 5), some new approaches introduce a more accurate study of the chemical and electrochemical effects both on the formation and dissolution of the barrier layer and on the nucleation and growth of the porous layer.[6,7] Information about the homogeneity and order of the porous alumina structure was obtained by analyzing the effect of the field strength, the electrolyte anions, the evolution of the electrolyte composition, and the temperature inside the pores.[8]

Experience has shown that it is difficult to obtain self-ordered and homogeneous alumina layers by one simple anodizing process. Nanoindentation or focused ion beam lithography of aluminum surfaces[9-11] had to be used to obtain perfect AAO geometries in a single process. However, larger highly ordered alumina layers can be obtained also by properly applying a two-step anodizing process.[12-14] In this procedure, the main parameter to control is the condition of the aluminum surface before the anodizing steps.

In this study, a two-step anodizing process in an oxalic acid electrolyte was analyzed. The experimental conditions for obtaining a homogeneous and ordered AAO were determined and the effect of the anodic applied voltage on the structure and geometry of the porous layer was studied. Symmetric (the same applied voltage in the two anodizing steps) and asymmetric assays (different applied voltages in the first and second anodizing step) were performed.

Experimental

Commercial sheets of 1050 aluminum alloy ($27 \times 27 \times 0.7$ mm) were used. The rough composition of AA1050 was a minimum of 99.5% Al, with Fe ($<0.30\%$) and Si ($<0.2\%$) as principal alloying elements.

The aluminum samples were treated before the anodizing process. The pretreatment was optimized in a previous study[15] and included five steps: alkaline degreasing in METEX T5-40A, alkaline etching in a NaOH/sodium gluconate solution 5:3 (w/w) at 55°C, desmutting in HNO_3 30% at room temperature, galvanostatic electropolishing in H_3PO_4/H_2SO_4 solution 3:2 at 70–80°C, and acid etching in H_3PO_4/CrO_3 3.5:2% at 55°C. Samples were thoroughly rinsed in double-distilled water after each step.

A potentiostatic two-step anodizing process in 0.30 M oxalic acid electrolyte (reagent grade in double-distilled water) at 20°C was studied. Immediately after the pretreatment, aluminum sheets were anodized (referred to as 1AN) in the oxalic acid bath under specified conditions. In a second step, the alumina layer was stripped (referred to as ST) in a standard H_3PO_4/CrO_3 3.5:2% solution. It was established that the time (in minutes) needed for optimum stripping of the layer was twice the thickness of the alumina layer (in μm).[15] Immediately after ST, a second anodizing process (referred to as 2AN) was carried out under specified conditions. Finally, samples were thoroughly rinsed in double-distilled water, air dried, and stored under vacuum.

A two-electrode thermostatized cell with a cylindrical lead cathode and agitation by air was used in the anodizing process. A power supply (250 V, 1 A) from Grelco Inc. (model GE2501DVG) was used to control the applied voltage, a microvoltmeter HP34401A was used to measure and transfer the registered current data to a computer, and a cryostat from Polyscience Inc. (model 9106) was used to adjust and control the bath temperature (accuracy of ±0.2°C).

The thickness of the alumina film (μm) was measured by the Eddy current method (Dualscope-Fischer Inst.).

Characterization of the morphology and geometry of the porous layer.— Field-emission scanning electron microscopy (FE-SEM) (Hitachi S-4100FE) and atomic force microscopy (AFM) (Multimode from Digital Instruments-Veeco) techniques were used in this study. On-top (the outer surface of the anodic layer and the aluminum substrate) and on-bottom (the inner surface of the oxide layer)

* Electrochemical Society Active Member.
z E-mail: c.muller@ub.edu

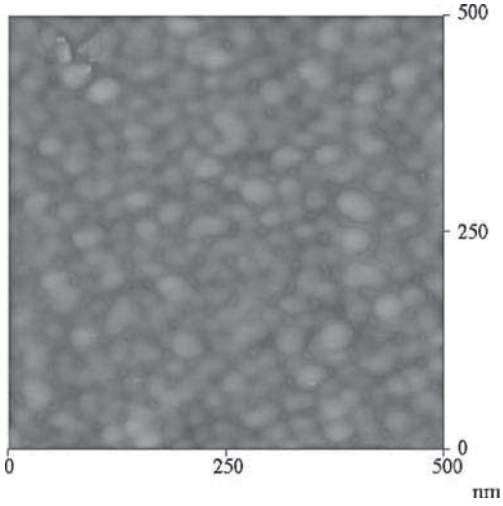

Figure 1. AFM image of the aluminum surface (roughness 1.2 nm) after electropolishing + acid etching.

viewings were carried out to study the porous AAO morphology and the state of the aluminum surface at different steps in the anodizing process.

The on-bottom preparation was carried out by a modified chemical-etching procedure.[16] As the aluminum samples were anodized on both sides, one side was etched with a concentrated NaOH solution. The remaining AAO layer was then protected with a lacquer and the exposed aluminum was etched in a solution containing $CuCl_2$/HCl until the alumina membrane was visible. To observe the on-bottom porous AAO structure, the barrier layer was etched by immersion in a H_3PO_4 2% solution (the etching time had to be accurately controlled). Finally, the lacquer was dissolved with ketone.

Different cell parameters of the resulting alumina were estimated by statistical calculations. The parameter that is commonly used to characterize the porous AAO structure is the interpore distance. However, this was difficult to measure in some cases. Therefore, measurements of pore and cell density and diameter (δ_{pore}, δ_{cell}, d_{pore}, and d_{cell}) were used. Using the program Digital Micrograph 3.7.0, the pore number and diameter were calculated from an SEM image with an area of 4.25 μm^2. A Gaussian adjustment was applied to obtain the average pore diameter from the distribution graph (pore number vs pore diameter). Sigmoidal adjustment was applied to calculate the pore density from the accumulative graph (accumulative pore number vs pore diameter) and the image area. As the ratio of pores/number of cells was greater than 1 in some cases, another parameter was defined to characterize the porous structure. This was the pore/cell density ratio. The cell diameter was calculated by assuming that the cells were circular with an area equal to $\pi \cdot (d_{cell}/2)^2$, and the cell density was inversely proportional to the cell area. The following equation, including the unity conversion agreement, was used

$$d_{cell}/\text{nm} = \sqrt{\frac{4 \times 10^6}{\pi \cdot \delta_{cell}(\mu m^{-2})}}$$

Results and Discussion

Preparation of an ordered AAO layer in a two-step anodizing process.— The order and homogeneity of pores in the AAO layer obtained after a single anodizing process depend on the conditions of the anodizing but also on the pretreatment of the aluminum surface.[15,17] The experimental conditions to obtain an appropriate pretreatment for the AA1050 samples were determined previously.[15]

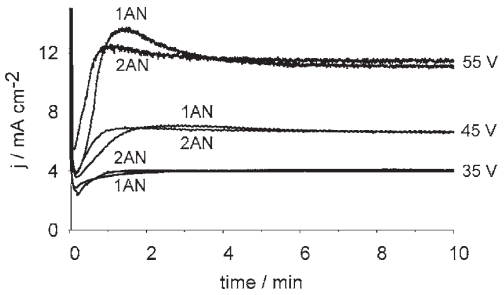

Figure 2. 1AN–2AN current density vs the time curves registered during the two-step potentiostatic aluminum anodizing process in oxalic acid 0.30 M at 20°C for 35, 45, and 55 V.

After this pretreatment, nonpatterned specular aluminum surfaces were obtained (Fig. 1), which induced the formation of a compact barrier layer in the first step of anodizing and the homogeneous nucleation of pores after the breakdown.

After a suitable pretreatment, the geometry and ordering of the layer obtained in a potentiostatic anodizing process is also a function of the applied voltage.[13,18] Figure 2 shows the j vs t curves obtained in potentiostatic anodizing processes at different applied voltages (1AN: first or single-step anodizing). In all cases, the current density initially decreased as a result of the formation of the barrier alumina layer. After the breakdown of the barrier layer, nucleation and the growth of pores took place and the current increased (a minimum current value appeared) until stationary conditions were attained. The time and the current density of this minimum value (j_{min}), the stationary current-density plateau, and the structure and geometry of the porous layer were directly related to the applied voltage. For instance, higher applied voltages led to higher stationary currents, as well as higher ($j_{statinary}$–j_{min}) and more uniform and ordered pore distributions. In these experiments, ordering was achieved by domains. Defects were accumulated at the edges of these domains, as observed in Ref. 19 and 20. However, single-step anodizing was not sufficient to produce a homogeneous ordered structure throughout the entire layer. In one-step samples, the structure of the alumina porous layer became ordered along the anodizing process. Thus, the SEM micrographs of the porous alumina layer formed at the end of the process (visible with an on-bottom view) showed more ordered structures than those of the layer formed at the beginning of the anodizing (on-top view) (Fig. 3).

In order to enhance the ordering and homogeneity of the porous

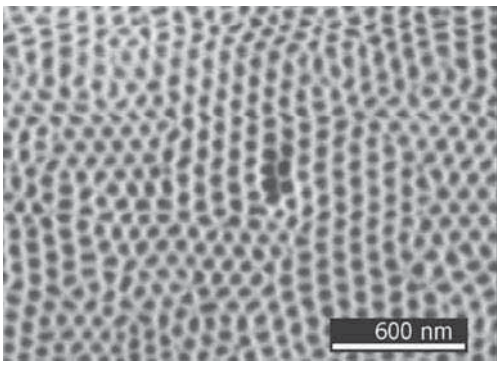

Figure 3. On-bottom SEM image of the alumina layer after a single-step anodizing process at 45 V.

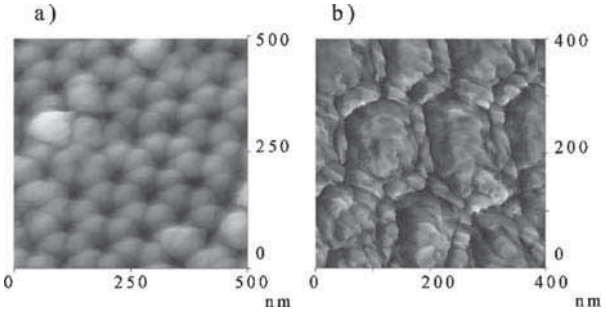

Figure 4. AFM images of (a) the aluminum surface after 1AN + ST, E_{1AN} = 45 V, and (b) on-bottom view of a 1AN barrier layer after Al substrate etching, E_{1AN} = 55 V.

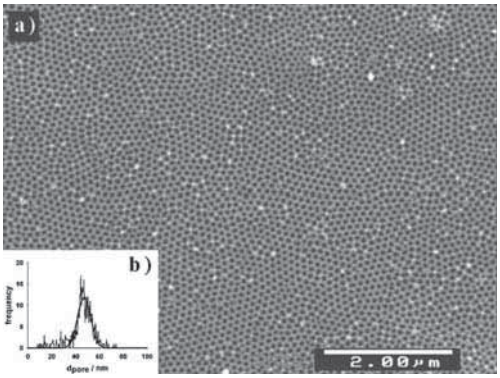

Figure 5. (a) On-top SEM image of the alumina layer after two-step potentiostatic anodizing at 45 V in oxalic acid 0.30 M at 20°C; (b) pore diameter distribution and Gaussian fit curve.

layer, a second anodizing step was applied. To undertake this two-step process, the first anodizing layer has to be chemically etched before applying the second layer (ST step).

Figure 2 shows that when the same bath, voltage, and time conditions were used, the initial steps in the anodizing process (barrier layer formation and pore nucleation) were different in the 1AN and 2AN processes. However, the same stationary j values were attained. Moreover, the differences observed after short times were enhanced by increasing the anodizing voltage. These differences between 1AN and 2AN were related to the formation of a nanoimprinted surface on aluminum after the stripping step. AFM images show that a hexagonal pattern was left on the aluminum surface (Fig. 4a) after 1AN and ST, and this was the same geometric structure observed in the 1AN barrier layer (on-bottom view in Fig. 4b). Therefore, this nanoimprinted surface induced the formation of a more ordered and homogeneous layer from the beginning of the 2AN process. By selecting the appropriate experimental parameters, homogeneous and ordered porous AAO layers were obtained for AA1050 that could be directly characterized by on-top viewing (Fig. 5).

Effect of the applied anodizing voltage.— Once the benefits of a second anodizing process had been verified, a systematic study was performed to analyze the effect of the applied voltage on the structure and geometry of the porous alumina layer obtained after a two-step anodizing process. The two-step potentiostatic experiments were classified into two groups: symmetric (the same applied voltage in 1AN and 2AN, $E_{1AN} = E_{2AN}$) and asymmetric (different applied voltages in 1AN and 2AN, $E_{1AN} \neq E_{2AN}$) (Table I). Single-step potentiostatic experiments at different voltages, followed by stripping of the AAO layer, were also performed to correlate the final results with characteristics of the aluminum surface before the application of the 2AN process.

Symmetric two-step potentiostatic experiments.— As indicated previously, when the same anodizing voltage was applied in 1AN and 2AN (experiments 1, 4, and 7, Table I), the short-time processes changed but the stationary current was very similar in the two steps (Fig. 2). Consequently, layer thicknesses were comparable and depended linearly on the applied voltage (Table I). In these experiments, the ordering and size of the hexagonal cells and the diameter of the pores in the layer obtained in the second anodizing process were controlled by the anodic voltage. At higher voltages, more regular structures were obtained with larger cell and pore diameters (Table I, Fig. 6), which is in agreement with data from previous studies.[8,21,22]

To analyze the influence of the pretreated aluminum surface on the performance of the single anodizing process, the correlation between the structure of the aluminum surface after stripping the 1AN layer and the geometry of the 2AN porous layer was examined. The AFM images in Fig. 7 show the pattern left on the aluminum surface after 1AN at 35, 45, and 55 V and stripping. Table I (experiments 8, 9, and 10) summarizes the pattern parameters obtained from these micrographs. A comparison of these results with those obtained after symmetric two-step anodizing (experiments 1, 4, and 7 in Table I)

Table I. Applied voltage and geometric parameters of the porous AAO layer obtained in a two-step anodizing process (experiments 1–7) and the aluminum pattern remaining after stripping the AAO layer obtained in a single-step anodizing process (experiments 8–10). Last column shows the thickness of the AAO layer measured after the 1AN and 2AN steps.

Experiment porous layer	E_{1AN} (V)	E_{2AN} (V)	d_{cell} (nm)	d_{pore} (nm)	δ_{pore} (μm^{-2})	Thickness (μm) (1AN-2AN)
1	35	35	102 ± 5	37 ± 7	123 ± 12	5.05 – 5.36
2	35	45	105 ± 6	35 ± 5	117 ± 12	7.99 – 13.50
3	35	55	97 ± 4	30 ± 5	137 ± 13	5.59 – 18.10
4	45	45	130 ± 9	46 ± 6	76 ± 11	10.30 – 9.39
5	55	35	151 ± 19	18 ± 7	δ_{cell}: 57 ± 14 δ_{pore}: 165 ± 55	20.00 – 5.35
6	55	45	165 ± 14	22 ± 8	δ_{cell}: 47 ± 4 δ_{pore}: 118 ± 24	18.60 – 10.30
7	55	55	155 ± 15	54 ± 7	54 ± 10	16.90 – 16.00
AFM Al pattern						
8	35	—	105 ± 6	60 ± 9	115 ± 13	
9	45	—	144 ± 11	95 ± 9	61 ± 9	
10	55	—	163 ± 22	109 ± 12	48 ± 13	

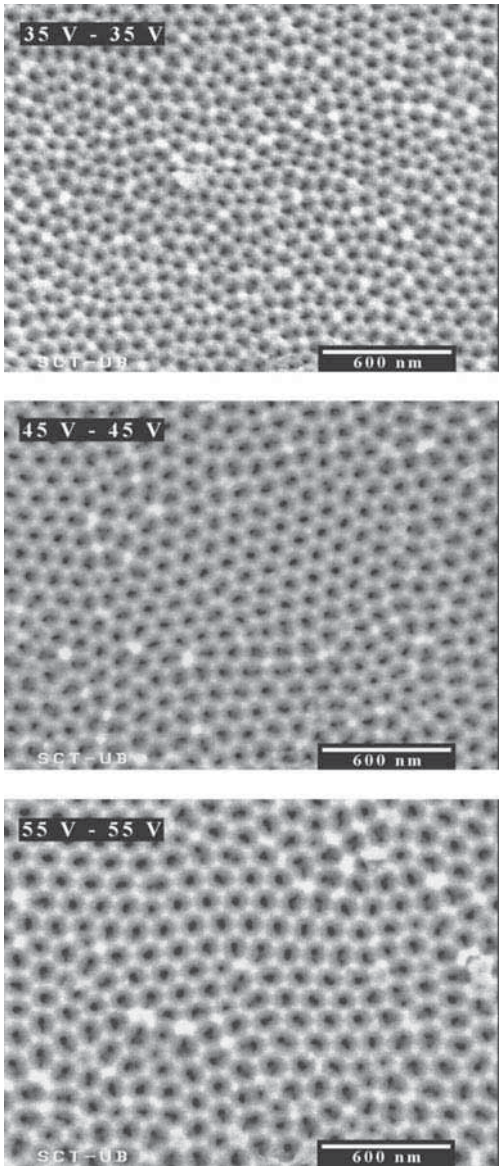

Figure 6. On-top SEM images of the alumina layer after symmetric two-step potentiostatic anodizing processes at different voltages.

revealed that the cell dimensions from the pattern were maintained during 2AN. However, the pore diameter measured on the aluminum pattern was usually larger than that found in the on-top view of the 1AN AAO porous layer previous to etching. This may be because the diameter measured on the Al substrate surface depended on etching parameters and consequently, did not correspond exactly to the base of the alumina pore. Nevertheless, the same tendency was observed in both cases: the higher E_{1AN}, the larger the pore diameter.

Asymmetric two-step potentiostatic experiments.— Three series with variable E_{1AN} and fixed E_{2AN} (35-2AN, 45-2AN, and 55-2AN series) and two series with fixed E_{1AN} and variable E_{2AN} (35-1AN and 55-1AN series) were carried out. Figure 8 and Table I show the micrographs and geometric parameters of the 2AN porous AAO layer obtained in these experiments.

An analysis of the pattern of the AAO layer revealed that different cell parameters were obtained when the E_{1AN} was varied but the 2AN voltage was kept constant [Table I, experiments 2, 4, and 6 (45-2AN series) and 3 and 7 (55-2AN)]. The values of the cell parameters were determined by E_{1AN}, because they coincided with the parameters measured in the imprinted Al surface after 1AN stripping or with the parameters in symmetric experiments at the same E_{1AN}. The stabilization currents obtained in these experiments were the same in all cases (Fig. 9), showing that the stationary current density was controlled by the voltage applied in the 2AN process. This behavior verified that the final thickness of the AAO layer depended on the applied 2AN voltage (Table I).

Similar cell parameters were obtained for a fixed E_{1AN} independently of the E_{2AN} (first row in Fig. 8 and 35-1AN and 55-1AN series from Table I). However, Fig. 10 shows that the stationary currents, the related thickness of the AAO layer, and the initial stages were very different in each E_{2AN}. Despite this, cell parameters only depended on E_{1AN}, as observed in the previous set of experiments (Table I).

An interesting result was obtained in relation to the diameter and density of pores. When E_{1AN} was the same or lower than E_{2AN}, the geometry of the pores matched that obtained in symmetric experiments. The cell parameters depended on the magnitude of the E_{1AN} voltage. However, if E_{1AN} was higher than E_{2AN}, the pore diameter was lower than expected (20 nm instead of 55 nm at E_{1AN} = 55 V) and the pore density was higher than the cell density. On-top SEM micrographs of the AAO layer obtained in the two-step anodizing process at E_{1AN} = 55 V and E_{2AN} = 35 or 45 V (Table I, experiments 5 and 6) show that more than one pore per cell was formed (Fig. 11). Therefore, cells with the same diameter (fixed by the E_{1AN}) but more pores per cell (fixed by the E_{2AN}) grew during the whole 2AN step. After a pore-enlargement post-treatment with phosphoric acid, these pores joined to form a unique pore per cell. A new parameter was then defined to characterize these structures: the pore/cell density ratio, which reached values of between 2 and 3. It was observed that this parameter increased as the difference between E_{1AN} and E_{2AN} increased. This type of geometry appeared when the cell diameter (determined by E_{2AN}) was less than that previously defined after stripping the 1AN layer (namely, when $E_{2AN} \leqslant E_{1AN}$).

Results show that the effect of E_{2AN} on the pattern (cell dimensions) of the porous AAO layer is negligible. However, the pore/cell density is modified by the ratio E_{2AN}/E_{1AN} and the electrochemical

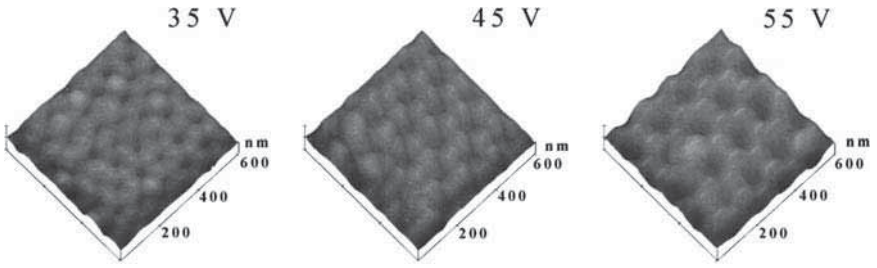

Figure 7. AFM images of the aluminum surface after single-step potentiostatic anodizing at different voltages (35, 45, and 55 V) + stripping in H_3PO_4/CrO_3

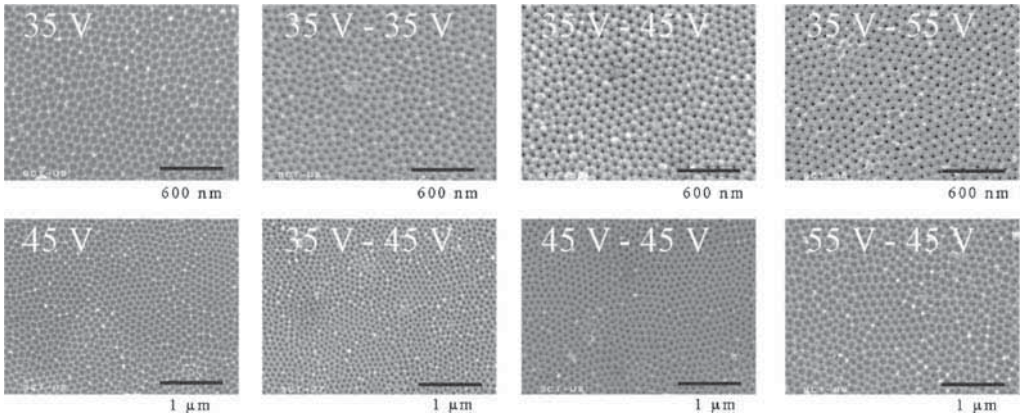

Figure 8. On-top SEM images of the aluminum surface (first column) and alumina layer (the rest of columns) showing the influence of voltages in the asymmetric two-step potentiostatic anodizing process

response in the 2AN process, including the stationary anodic current and the corresponding AAO layer thickness, was defined by the E_{2AN}.

Conclusions

This study demonstrates that, under the appropriate conditions, a two-step anodizing process can lead to uniform, ordered, and homogeneous alumina porous structures on 1050 aluminum alloy sheets.

The influence of voltage on the alumina structure obtained in the two-step potentiostatic anodizing process was studied. Overall results show that:

1. When the same voltage was applied in the 1AN and 2AN steps (symmetric anodizing), the cell parameters varied as expected. Higher voltages resulted in larger cell and pore diameters.
2. When different voltages were applied in the 1AN and 2AN steps (asymmetric anodizing), the cell parameters varied as expected

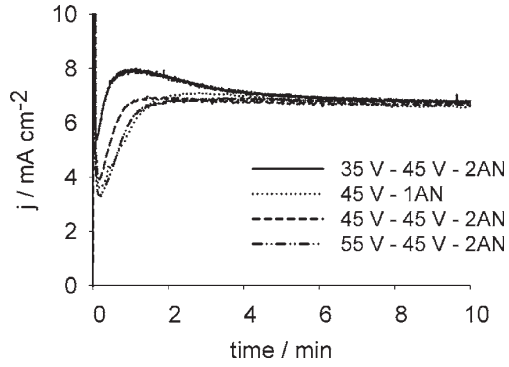

Figure 9. j vs t curves corresponding to asymmetric two-step potentiostatic anodizing processes in oxalic acid 0.30 M at 20°C: E_{2AN} = 45 V and different E_{1AN} voltages and a single-step anodizing process at 45 V as a reference.

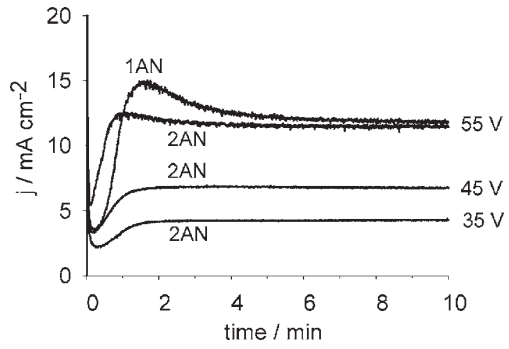

Figure 10. j vs t curves corresponding to asymmetric two-step potentiostatic anodizing processes in oxalic acid 0.30 M at 20°C: E_{1AN} = 55 V and E_{2AN} = 35, 45, or 55 V.

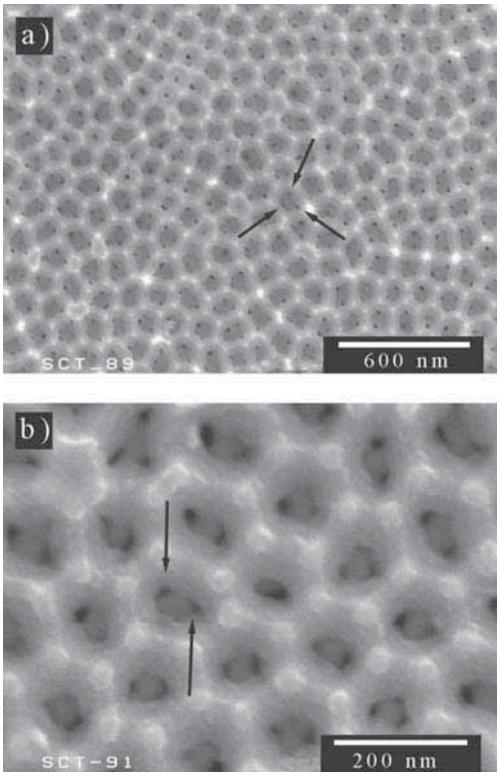

Figure 11. On-top SEM images of the alumina layer after asymmetric two-step anodizing processes. Arrows show more than 1 pore per cell when E_{1AN} is higher than E_{2AN}: (a) E_{1AN} = 55 V, E_{2AN} = 35 V; (b) E_{1AN} = 55 V, E_{2AN} = 45 V.

in the function of the first anodizing voltage. The second voltage had little influence. As in the symmetric conditions, larger cell diameters were obtained at higher first-anodizing voltages. In terms of pore dimensions, a special case was found when the first anodizing voltage was higher than the second one. In this case, the pore/cell ratio was greater than 1, resulting in a structure with more than one pore per cell.

3. The cell parameters resulting from nanoimprinting of the aluminum surface after the first anodizing + stripping process explain the parameters found in the alumina porous layer after the second anodizing process.

Acknowledgments

The authors thank the Serveis Cientificotècnics (Universitat de Barcelona) for the use of their equipment. This paper was supported by the grant MAT 2003-09483 from the MEC. J. M. Montero thanks the DURSI for their financial support.

University of Barcelona assisted in meeting the publication costs of this article.

References

1. A. Huczko, *Appl. Phys. A*, **70**, 365 (2000).
2. M. Hernandez-Velez, *Thin Solid Films*, **495**, 51 (2005).
3. J. C. Hulteen and C. R. Martin, *J. Mater. Chem.*, **7**, 1075 (1997).
4. S. Inoue, S. Z. Chu, K. Wada, D. Li, and H. Haneda, *Sci. Technol. Adv. Mater.*, **4**, 269 (2003).
5. P. G. Sheasby and R. Pinner, *The Surface Treatment and Finishing of Aluminum and Its Alloys*, 6th ed., Vol. 1, p. 11, Finishing Publications Limited with ASM International (2001).
6. I. Vrublevski, V. Parkoum, J. Schreckenbach, and G. Marx, *Appl. Surf. Sci.*, **227**, 282 (2004).
7. I. Vrublevski, V. Parkoum, V. Sokol, and J. Schreckenbach, *Appl. Surf. Sci.*, **236**, 270 (2004).
8. G. Patermarakis and K. Masavetas, *J. Electroanal. Chem.*, **588**, 179 (2006).
9. K. Yasui, K. Nishio, H. Nunokawa, and H. Masuda, *J. Vac. Sci. Technol. B*, **23**, L9 (2005).
10. J. Choi, R. B. Wehrspohn, and U. Gösele, *Electrochim. Acta*, **50**, 2591 (2005); H. Masuda, K. Yasui, Y. Sakamoto, M. Nakao, T. Tamamura, and K. Nishio, *Jpn. J. Appl. Phys., Part 2*, **40**, L1267 (2001).
11. N. W. Liu, A. Datta, C. Y. Liu, and Y. L. Wang, *Appl. Phys. Lett.*, **82**, 1281 (2003).
12. H. Masuda and K. Fukuda, *Science*, **268**, 1466 (1995).
13. J. H. Yuan, F. Y. He, D. C. Sun, and X. H. Xia, *Chem. Mater.*, **16**, 1841 (2004).
14. G. D. Sulka, S. Stroobants, V. Moschchalkov, G. Borghs, and J. P. Celis, *J. Electrochem. Soc.*, **149**, D97 (2002).
15. J. M. Montero, M. Sarret, and C. Müller, *Surf. Coat. Technol.*, Accepted.
16. T. T. Xu, R. D. Piner, and R. S. Ruoff, *Langmuir*, **19**, 1443 (2003).
17. P. Bocchetta, C. Sunseri, R. Masi, S. Piazza, and F. Di Quarto, *Mater. Sci. Eng., C*, **23**, 1021 (2003).
18. G. D. Sulka and K. Parkola, *Thin Solid Films*, **515**, 338 (2006).
19. A. P. Li, F. Müller, A. Birner, K. Nielsch, and U. Gösele, *J. Appl. Phys.*, **84**, 6023 (1998).
20. O. Jessensky, F. Müller, and U. Gösele, *J. Appl. Phys.*, **72**, 1173 (1998).
21. H. Masuda, H. Yamada, M. Satoh, H. Asoh, M. Nakao, and T. Tamamura, *Appl. Phys. Lett.*, **71**, 2770 (1997).
22. S. Ono and N. Masuko, *Surf. Coat. Technol.*, **169–170**, 139 (2003).

Setting a self-ordered alumina template by two-step galvanostatic anodizing: nanotexturing and mechanism notions

Submitted to Electrochimica Acta

Setting a self-ordered alumina template by two-step galvanostatic anodizing: nanotexturing and mechanism notions

J.M. Montero-Moreno, M. Sarret, C.M. Müller
Electrodep (Departament de Química Física), Universitat de Barcelona, c/ Martí i Franquès 1 E-08028 Barcelona, Spain

Keywords:
Two-step anodizing
Galvanostatic
Self-ordered
Anodic aluminium oxide

A B S T R A C T

Galvanostatic two-step anodizing is not frequently used in the manufacture of alumina templates due to its unrestrained voltage. As a consequence, the evolution of structural parameters and the correlation between self-ordering, nanotexturing of the aluminium surface and operating conditions have received little attention in galvanostatic processes. Notwithstanding, the proper choice of the operating conditions in this method allows the tuning of self-ordering and control of burning. This paper reports the analysis of the effect of experimental conditions on galvanostatic two-step anodizing on AA1050, in order to obtain self-ordered alumina templates. Results show that, by accurate control, alumina membranes are obtained with a defined structure and order that are similar to those obtained with voltage-controlled anodizing.

1. Introduction

Anodizing is a complex process involving the formation of an anodic aluminium oxide (AAO) with a two-layered structure [1]. The porous layer consists of a hexagonal arrangement of cells with a central pore per cell that elongates from top to bottom of the layer, resembling a honeycomb. This feature has wide application in the synthesis of new 1D-nanomaterials with wired or tubular shapes by a template procedure [2-7]. In recent decades, it has been established that high-quality nanomaterials are obtained by this method if pores are well-defined and homogeneous. For this reason, the degree of ordering of these cell arrangements plays an important role and researchers have tried hard to understand this phenomenon [8-17]. In addition, the cell structure and ordering degree must be maintained throughout the whole layer, not just on top of AAO. Aluminium nanotexturing and self-ordered anodizing have become powerful tools in the manufacture of high-quality AAOs. Nanotexturing implies the fixation of pore nucleation sites by drawing a pattern over the aluminium surface by natural or synthetic approach [18-22], and self-ordering is a particular anodizing growth regime in which cells tend to re-organize themselves. This regime is well established in voltage-controlled anodizing, as the driving force is the electric field generated at the barrier layer [8]. Thus, voltage-controlled two-step anodizing has become a common method for producing AAO membranes, as it involves nanotexturing and controlled self-ordering [23, 24]. The correlation between the structure of the porous AAO and the operating conditions of the process is well established [1, 10, 11, 15, 25].

Galvanostatic anodizing is also interesting, as allows better control of local catastrophic phenomena and burning [13, 14]. However, it is not commonly used because of its uncontrolled voltage and, consequently, undefined cell parameters. Formation mechanism under constant current has been studied for many years [26-28], but at present self-ordering is unknown for this process and, thus, for the two-step anodizing procedure. The present study looks at galvanostatic two-step anodizing, and compares it with common voltage-controlled two-step anodizing. We focus on two aspects that are important to the control of the characteristics of the final alumina layer: first, the influence that experimental conditions applied in the first anodizing step have on the second step, by comparing structural parameters measured after each step; second, the analysis of the divergence in the formation processes of the AAO between voltage-controlled and galvanostatic two-step anodizing.

2. Experimental

Sheets of laminated 1050 aluminium (27 mm x 27 mm x 0.7 mm) were used in this study (Al >99.5%, Fe <0.30%, Si <0.20%). Samples were cleaned first in a degreaser solution (Metex T5-40A®) and then in an alkaline bath

($NaOH:C_6H_{11}O_7Na$). Oxides were removed in 30% HNO_3 and electropolishing was carried out with a H_3PO_4:H_2SO_4 bath at 75ºC. A final acid etching in H_3PO_4:CrO_3 was required to eliminate oxides formed during electropolishing [29].

Two-step anodizing was performed in oxalic acid under voltage (45 V) or current (3 - 10 mA·cm^{-2}) control. After a first anodizing, alumina was stripped in H_3PO_4:CrO_3. A second anodizing step was immediately carried out. Anodizing was performed in a thermostatted two-electrode cell with a lead cathode and agitation by air. We used combinations of different concentrations (0.30 - 0.60 M), temperatures (10 - 20ºC) and durations (30 - 180 min).

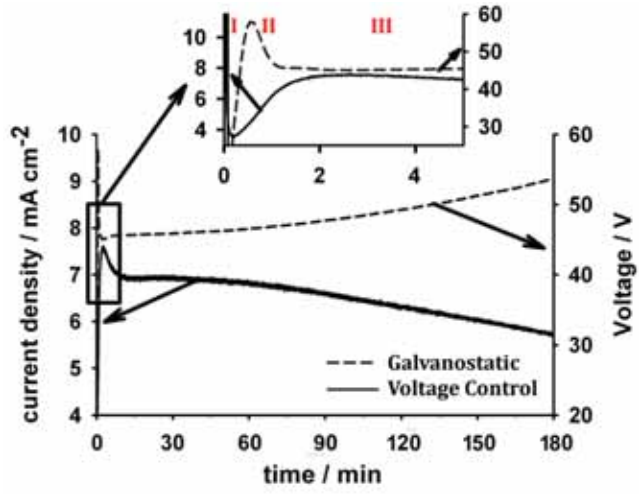

Figure 1: *j* and V *vs.* time plots (180 min) for voltage-controlled and galvanostatic first anodizing step (45 V, 0.30 M, 20 ºC and 10 mA·cm^{-2}, 0.60 M, 20 ºC, respectively).

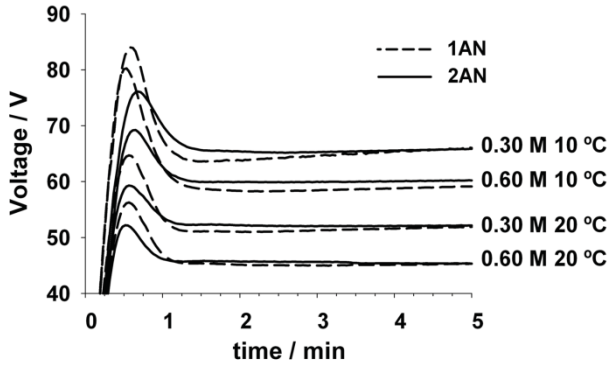

Figure 2: V–t plots for galvanostatic first (1AN) and second (2AN) two-step anodizing at different bath conditions (j = 10 mA·cm^{-2}, t_{1AN} and t_{2AN} = 60 min).

Thickness was measured by the eddy current method with a Dualscope FMP100 (Fischer). Samples were characterized by Atomic Force Microscopy (AFM) with a Veeco-Multimode Digital Instrument. Inter-pore distance (d_{int}) was measured from these images after first and second anodizing and after stripping of these layers. Thus, the evolution of d_{int} through the layer was calculated. Ordering degree was evaluated from on-top SEM images of final alumina membranes (FE-SEM Hitachi S-4100FE).

3. Results and discussion

3.1. Hints in the anodizing mechanism at constant current

Figure 1 shows the characteristic electrochemical response in galvanostatic (dash) and voltage-controlled (solid) anodizing. The mechanism of AAO formation could be monitored from these curves [1, 30]: growth of a compact alumina layer (I), breakdown of this layer and pore nucleation (II) and pore growth by field-assisted local dissolution [31, 32] (III). A peak-shaped curve was characteristic, followed by a long plateau, corresponding to pseudo-stationary conditions, whereas barrier layer thickness remained constant and porous layer thickened. This meant that there were balanced oxide formation and etching rates in the barrier layer, but not in the porous layer. However, after a long time (>60 min), electrolyte resistance inside the pores rose, causing a time-dependent grow of voltage [31]. The thickening of the AAO implied a longer path for ions to cover inside the pore. The same mechanism applied in the second anodizing, although some divergences were observed (Figure 2). Initial peaks were not so pronounced, indicating the existence of a nanotexture in the aluminium surface before the second anodizing (images I and III in Figure 3). This facilitated the nucleation of the pores, as hollows acted as preferential sites for initiation of field-assisted local dissolution. Consequently, breakdown of the initial layer proceeded at lower voltages. This nanotexture also explained why the degree of ordering was improved with a second anodizing process [29, 32, 33]. If no nanotexture was present on the surface, pores nucleated randomly and without a prefixed d_{int} (image II in Figure 3). However, when the surface was nanotextured, pores nucleated at the marked locations (image IV in Figure 3). Though nanotexturing was important in the obtaining of quality AAOs, the effect of self-ordering anodizing was more important if structural parameters were liked to be maintained throughout the whole layer. The presence of ordered domains of cells in the AFM images showed that self-ordering was working.

Charge values were gathered from galvanostatic and voltage-controlled experiments under various experimental conditions and, when plotted, a single linear relationship with thickness was obtained (eq. [a]), ranging from 5 to 50 μm. This indicated that etching of the porous layer by the acidic solution was negligible during anodizing for $t_{AN} \leq 180$ min and our conditions were far from the limit of the maximum AAO thickness (no balanced growth and etching rates of the porous layer). Confirming this assumption, on-top AFM images of the

AAO surface layer after a first anodizing (image II in Figure 3) show that the initial disordered structure was still visible after 180-minute anodization.

$$e(\mu m) = 0.45 \cdot Q\left(C \cdot cm^{-2}\right) + 0.52 \qquad [a]$$

Finally, a unique dependence of growth rate with current density was observed at steady-state conditions in both voltage and current controlled processes, showing that the electrical efficiency was the same: at a fix charge, the same thickness of the alumina layer was always obtained.

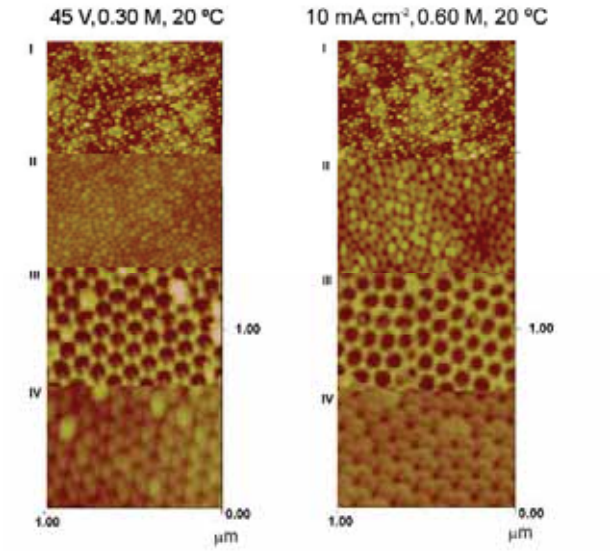

Figure 3: AFM images of aluminium and AAO surface at different stages of two-step galvanostatic and voltage-controlled anodizing. Images taken after (I) electropolishing, (II) 60-min first anodizing, (III) stripping of the first alumina layer, (IV) 60-min second anodizing.

3.2. Setting self-ordered galvanostatic anodizing

Two-step galvanostatic anodizing was assayed at different current densities and operating conditions (Table 1). It was found that self-ordering only occurred when $V_{plateau}$ was around 45 V, a voltage that matched the bibliographic data on self-ordered voltage-controlled anodizing in oxalic acid [14]. However, under galvanostatic conditions, $V_{plateau}$ can be modulated by the operating conditions: bath concentration and temperature could be tuned for each current density to set $V_{plateau}$ at 45 V. As a general rule, higher current densities required higher concentration or temperature to raise the desired voltage. In this study, current densities from 3 to 10 $mA \cdot cm^{-2}$ were assayed and experimental parameters were modulated to fix $V_{plateau}$ = 45 V. The AAOs obtained were similar in structure, even to the AAOs manufactured by two-step voltage-controlled anodizing at 45 V with concentration and temperature adjusted to set equivalent current density. No significant differences in thickness and d_{int} (Table 1) were measured. Self-ordering also worked (Figure 4), confirming that voltage (i.e. electric field) is the main factor in the ordering phenomenon, even in galvanostatic processes. The chance to tune self-ordering as a function of concentration and temperature for each current density introduced a degree of freedom for optimization of the process, in order to avoid burning or local catastrophic events at high current densities [13]. The influence of these operating conditions in the process was analyzed at 10 $mA \cdot cm^{-2}$, a current density in the upper limit of that registered in voltage-controlled anodizing in oxalic acid at 40 V (usually smaller than 6 $mA \cdot cm^{-2}$) [12, 30, 34].

Table 1

Inter-pore distances for different galvanostatic two-step anodizing (t_{1AN} and t_{2AN} = 60 min), as functions of current density, concentration and temperature.

j / $mA \cdot cm^{-2}$	T / ºC	C / M	d_{int} / nm	$V_{plateau}$ / V
3.1	10	0.30	119 ± 8	44 *
6.6	20	0.30	128 ± 10	45 *
10	20	0.60	123 ± 8	46 *
10	20	0.30	159 ± 16	53
10	10	0.60	167 ± 19	60
10	10	0.30	202 ± 33	67
10	25	0.30	122 ± 8	43*

* Self-ordering

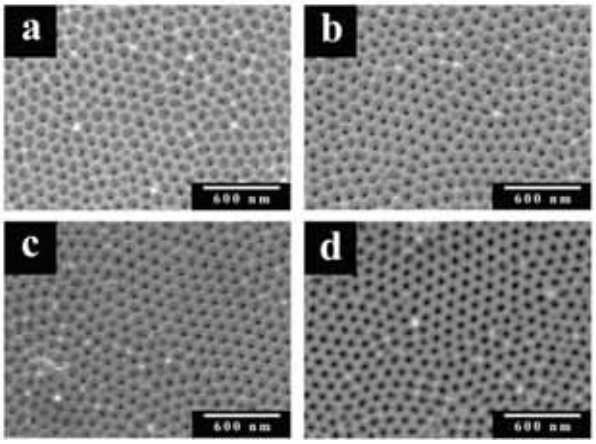

Figure 4: On-top SEM images of the AAO layer after two-step anodizing in 0.30 M oxalic acid (t_{1AN} and t_{2AN} = 60 min) at a) 3.1 $mA \cdot cm^{-2}$ and 10 ºC; b) 6.6 $mA \cdot cm^{-2}$ and 20 ºC; c) 45 V and 10 ºC; d) 45 V and 20 ºC.

3.3. Effect of bath concentration and temperature

The influence of electrolyte concentration and bath temperature on d_{int} and ordering degree was analyzed at a fixed current density (10 $mA \cdot cm^{-2}$). It was found that, as expected, d_{int} ranged between 115 and 170 nm depending on conditions (Table 1), due to the correlation between $V_{plateau}$ and the

operating conditions (Figure 2). As in [8], higher voltages and d_{int} were measured at lower temperatures and concentrations (Table 1 and Figure 5). This behaviour indicated a relationship between the electric field generated in the barrier layer (i.e. voltage drop in the barrier layer) and bath chemistry, as observed with other bath types (sulphuric acid, phosphoric acid etc.). Stronger acids and higher temperatures and concentrations affected barrier layer thickness by increasing the etching rate at the pore bottom. In consequence, the electric fields in the barrier layer decreased and subsequently the voltage dropped.

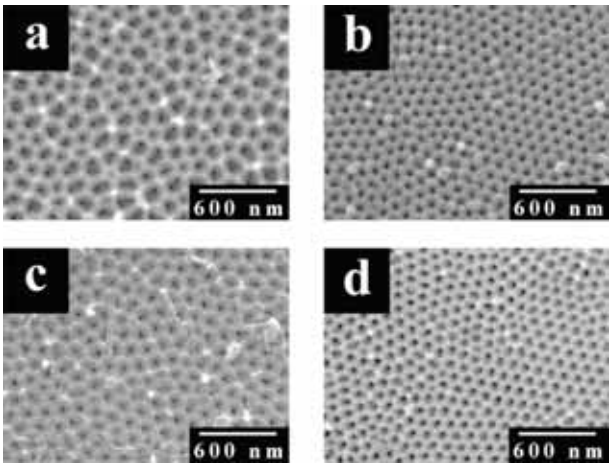

Figure 5: On-top SEM images of porous AAO after galvanostatic (10 $mA \cdot cm^{-2}$) two-step anodizing (t_{1AN} and t_{2AN} = 60 min) in oxalic acid bath, showing the influence of electrolyte concentration and bath temperature: a) 10 ºC, 0.30 M; b) 25 ºC, 0.30 M; c) 10 ºC, 0.60 M; d) 20 ºC, 0.60 M.

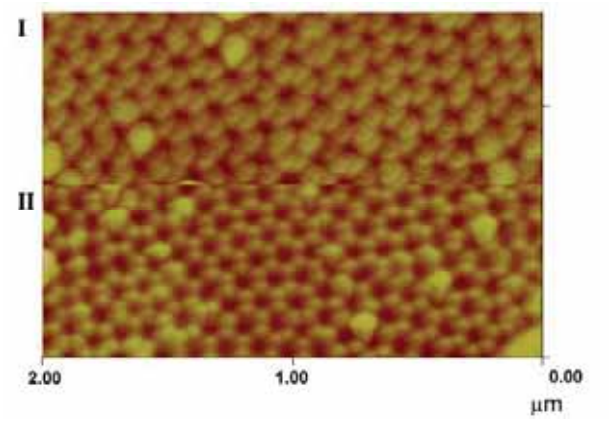

Figure 6: AFM image of the aluminium surface after (I) 180-min first anodizing and stripping, (II) 60-min second anodizing and stripping. Anodizing was carried out galvanostatically at 10 $mA \cdot cm^{-2}$, 0.60 M oxalic acid and 20 ºC.

Self-ordering appeared in all the experiments when $V_{plateau}$ = 45 V (Table 1 and Figure 5), showing the versatility of this approach. In a similar way, Almasi-Kashi and co-workers [11] claimed that self-ordering in voltage-controlled anodizing is not only limited to voltage, but also extends to a range of temperatures (minimum and maximum) that can be tailored by bath concentration. Nevertheless, the range of experimental conditions which can be applied to modulate the voltage at each applied current density is limited by solubility, conductivity and mass transport properties.

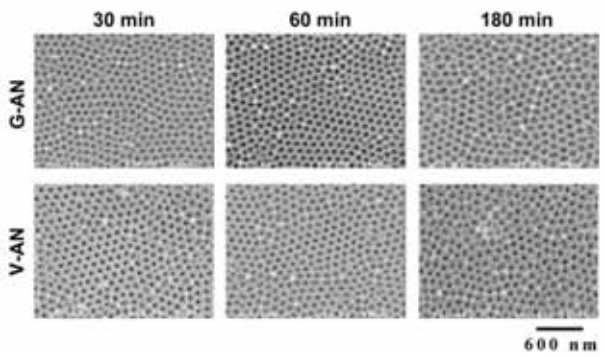

Figure 7: On-top SEM images of porous AAO after two-step anodizing in 0.30 M oxalic acid bath at 20 ºC, showing the effect of t_{1AN}: 30, 60 and 180 min. t_{2AN} = 60 min. G-AN: galvanostatic at 10 $mA \cdot cm^{-2}$. V-AN: voltage-controlled at 45 V.

3.4. Dependence of AAO structure on first anodizing time

Self-ordered galvanostatic two-step anodizing was carried out at different first anodizing times (30 min < t_{1AN} < 180 min) and a constant 60-minute second step. In AFM images of the aluminium surface and on-top SEM images of the AAO layer, correlation of d_{int} and ordering degree was seen as a function of time. If t_{1AN} <60 minutes (plateau state), constant d_{int} was recorded after the second anodizing (115 ± 5 nm). If longer anodizings were carried out, pseudo-stationary conditions were overtaken, driving to higher d_{int} (140 ± 5 nm for t_{1AN} = 180 min). Voltage plot in Figure 1 revealed that this change in d_{int} was, in fact, related to the voltage recorded at the end of the first anodizing step. For t_{1AN} <60 minutes, the system was still at plateau conditions, with voltage ~ 46 V, matching the measured d_{int} with the expected value for this voltage. Longer anodizing gave higher final voltages, up to 54 V after 180 minutes, due to the increased resistance of the layer. Consequently, an enlargement of d_{int} at the bottom of the first anodic layer was observed on the AFM image of the aluminium surface that remained after it was stripped (Figure 6-I), which corroborated the expected relationship between voltage and d_{int} [8]. Nevertheless, this d_{int} was lost after a 60-minute second anodizing throughout the whole layer, as the surface texture of the aluminium revealed after the second AAO layer was stripped (Figure 6-II). This shows that the geometry of the AAO layer is limited by the anodizing time in galvanostatic processes, but that the order and dimensions of

the cells can be recovered after a short second anodizing process.

In addition, on-top SEM images of the AAO layer obtained after two-step anodizing shows that the duration of the first anodizing modifies the order of the final structure (Figure 7). Although at t_{1AN} >60 min., ordering improved, increasing the first anodizing time, which confirmed results reported by other researchers [10, 25, 32], at longer times ordering started to decrease (the ordering had nearly disappeared after a 180-minute anodizing). This phenomenon was explained as an effect of inter-metallic compounds enclosed in the aluminium matrix (AA1050). While anodizing, they became incorporated into the AAO and disrupted the homogeneous development of pores (Figure 8). At the beginning the effect was slight, but after a time the amount of these particles inside the AAO increased. A competition between the self-ordering and the disordering caused by this particle took place, clarifying the previous observations.

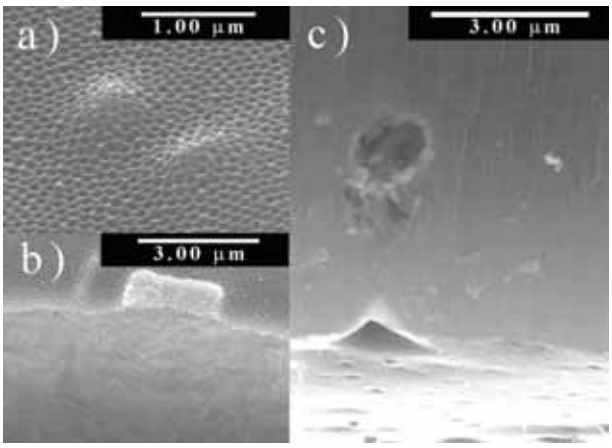

Figure 8: a) On-top view of the effect of inner inter-metallic compounds on the surface of the porous AAO layer. b) Cross-section of an inter-metallic compound placed on the surface of the porous AAO layer. c) Cross-section of an AAO layer after the aluminium was etched, showing the effect of an inter-metallic compound on the barrier layer side.

4. Conclusions

Self-ordering was possible for galvanostatic anodizing in oxalic acid bath. To achieve high-quality membranes, two-step galvanostatic anodizing was applied and the structures obtained were compared with those obtained with voltage-controlled anodizing. It was demonstrated that, although the galvanostatic approach is time limited to the extent of the voltage plateau, the self-ordering conditions can be attained at different values of concentration (c) and temperature (T) without any change in the thickness of the alumina layer (electrical efficiency). Nevertheless, only one experimental setup (c,T) allow us to obtain the self-ordering conditions and the same growth rate (thickness) of the alumina layer in a voltage-controlled approach. This behaviour can be useful to modulate the growth of a self-organized alumina layer on a nanoindented aluminium surface and controlling the burning phenomenon.

Acknowledgments

This paper was supported by contract MAT2006-12913 from the Spanish Ministry of Science and Innovation. J.M. Montero acknowledges the Comissionat per a Universitats i Recerca of the Departament d'Innovació, Universitats i Empresa of the Generalitat de Catalunya and the Fons Social Europeu for financial support. The authors wish to thank the Serveis Cientificotècnics of the University of Barcelona for use of their equipment.

References

[1] P.G. Sheasby, R. Pinner, The Surface Treatment and Finishing of Aluminum and its Alloys, 2001.
[2] A. Huczko, Appl. Phys. A-Mater 70 (2000) 365.
[3] M. Hernández-Vélez, Thin Solid Films 495 (2006) 51.
[4] J.C. Hulteen, C.R. Martin, J. Mater. Chem. 7 (1997) 1075.
[5] S. Inoue, S.-Z. Chu, K. Wada, D. Li, H. Haneda, Sci. Technol. Adv. Mat. 4 (2003) 269.
[6] C.Y. Han, Z.L. Xiao, H.H. Wang, G.A. Willing, U. Geiser, U. Welp, W.K. Kwok, S.D. Bader, G.W. Crabtree, Plat. Surf. Finish. 91 (2004) 40.
[7] G. Sauer, G. Brehm, S. Schneider, K. Nielsch, R.B. Wehrspohn, J. Choi, H. Hofmeister, U. Gosele, J. Appl. Phys. 91 (2002) 3243.
[8] A.P. Li, F. Muller, A. Birner, K. Nielsch, U. Gosele, J. Appl. Phys. 84 (1998) 6023.
[9] M.T. Wu, I.C. Leu, M.H. Hon, J. Vac. Sci. Technol. B 20 (2002) 776.
[10] B. Lu, S. Bharathulwar, D.E. Laughlin, D.N. Lambeth, J. Appl. Phys. 87 (2000) 4721.
[11] M. Almasi-Kashi, A. Ramazani, J. Phys. D Appl. Phys. 38 (2005) 2396.
[12] M.T. Wu, I.C. Leu, M.H. Hon, J. Vac. Sci. Technol. B 22 (2004) 2326.
[13] S. Ono, M. Saito, M. Ishiguro, H. Asoh, J. Electrochem. Soc. 151 (2004) B473.
[14] S. Ono, M. Saito, H. Asoh, Electrochim. Acta 51 (2005) 827.
[15] G.D. Sulka, K.G. Parkola, Thin Solid Films 515 (2006) 338.
[16] S. Mátéfi-Tempfli, M. Mátéfi-Tempfli, L. Piraux, Thin Solid Films 516 (2008) 3735.

[17] O. Jessensky, F. Muller, U. Gosele, Appl. Phys. Lett. 72 (1998) 1173. [18] L. Zhang, H.S. Cho, F. Li, R.M. Metzger, W.D. Doyle, J. Mater. Sci. Lett. 17 (1998) 291.
[19] N.W. Liu, A. Datta, C.Y. Liu, Y.L. Wang, Appl. Phys. Lett. 82 (2003) 1281.
[20] H. Masuda, H. Asoh, M. Watanabe, K. Nishio, M. Nakao, T. Tamamura, Adv. Mater. 13 (2001) 189.
[21] H. Masuda, Y. Matsui, M. Yotsuya, F. Matsumoto, K. Nishio, Chem. Lett. 33 (2004) 584.
[22] H. Masuda, H. Yamada, M. Satoh, H. Asoh, M. Nakao, T. Tamamura, Appl. Phys. Lett. 71 (1997) 2770.
[23] H. Masuda, K. Fukuda, Science 268 (1995) 1466.
[24] G.D. Sulka, S. Stroobants, V. Moshchalkov, G. Borghs, J.P. Celis, J. Electrochem. Soc. 149 (2002) D97.
[25] H. Masuda, K. Yada, A. Osaka, Jpn. J. Appl. Phys. 2 37 (1998) L 1340.
[26] V.P. Parkhutik, Corros. Sci. 26 (1986) 295.
[27] G. Patermarakis, K. Masavetas, J. Electroanal. Chem. 588 (2006) 179.
[28] I. Vrublevsky, V. Parkoun, V. Sokol, J. Schreckenbach, G. Marx, Appl. Surf. Sci. 222 (2004) 215.
[29] J.M. Montero-Moreno, M. Sarret, C. Müller, Surf. Coat. Tech. 201 (2007) 6352.
[30] F. Li, L. Zhang, R.M. Metzger, Chem. Mater. 10 (1998) 2470.
[31] G. Patermarakis, K. Moussoutzanis, Electrochim. Acta 40 (1995) 699.
[32] M. Ghorbani, F. Nasirpouri, A. Iraji zad, A. Saedi, Mater. Design 27 (2006) 983.
[33] J.M. Montero-Moreno, M. Sarret, C. Müller, J. Electrochem. Soc. 154 (2007) C169.
[34] I. Vrublevsky, V. Parkoun, J. Schreckenbach, G. Marx, Appl. Surf. Sci. 220 (2003) 51.

Assessment of the thermal stability of anodic alumina membranes at high temperatures

Materials Chemistry and Physics 111 (2008) 542–547

Contents lists available at ScienceDirect

Materials Chemistry and Physics

journal homepage: www.elsevier.com/locate/matchemphys

Assessment of the thermal stability of anodic alumina membranes at high temperatures

L. Fernández-Romero[a], J.M. Montero-Moreno[b], E. Pellicer[a,*], F. Peiró[a], A. Cornet[a], J.R. Morante[a], M. Sarret[b], C. Müller[b]

[a] Enginyeria i Materials Electrònics (EME/CEMIC/CeRMAE), Departament d'Electrònica, Facultat de Física, Universitat de Barcelona, C/ Martí i Franquès, 1, E-08028 Barcelona, Spain
[b] Laboratori d'Electrodeposició i Corrosió (Electrodep), Departament de Química Física, Facultat de Química, Universitat de Barcelona, C/ Martí i Franquès, 1, E-08028 Barcelona, Spain

ARTICLE INFO

Article history:
Received 13 December 2007
Received in revised form 28 April 2008
Accepted 7 May 2008

Keywords:
Aluminium oxide
AA1050
Electrochemical techniques
Annealing
X-ray diffraction

ABSTRACT

The thermal stability of anodic alumina membranes (AAMs) annealed in air from 750 °C up to 1100 °C was investigated. AAMs were produced by single-step anodising of laminated AA1050 in 0.30 M oxalic acid medium. The barrier layer provided thermal stability to the membranes, since it avoided or minimized bending and cracking phenomena. X-ray diffraction (XRD) analyses revealed that as-synthesized AAMs were amorphous and converted to polycrystalline after heat-treating above 750 °C. However, porous and barrier layers did not re-crystallize in the same way. The porous layer mainly crystallized in the γ-Al_2O_3 phase within the range of 900–1100 °C, while the barrier layer was converted to the α-Al_2O_3 phase at 1100 °C. Different grain sizes were also estimated from Scherrer's formula. Scanning electron microscopy (SEM) images pointed out that cell wall dilation of the porous layer explained membrane cracking, which was avoided in presence of the barrier layer.

1. Introduction

Anodic alumina membranes (AAMs) have received a lot of attention because of their unique structural properties provided by a uniform and parallel porous structure [1–7]. AAMs are known to have narrow size distribution for pore diameters and interpore distances, which make them an ideal template for the fabrication of highly ordered fibrils, rods, wires, and tubules of metals, semiconductors and other solid materials. Moreover, the fabrication of porous alumina on silicon substrates for the synthesis of nanoengineered structures integrated with electronic and optoelectronic devices is the object of several investigations [8–10]. Producing AAMs is also of great interest since precision microcomponents from refractory materials are required for numerous applications, such as microsensor devices [11,12]. Microsensor applications usually involve operating at high temperatures and thus, stability to thermal shocks is a technological requirement.

The two-layered structure (porous layer–barrier layer) of anodised alumina is the outcome of the combination of different processes that take place during the electrochemical oxidation of aluminium [13]. During anodising, firstly, a compact layer of aluminium oxide is formed on the surface. The high electric resistance of this layer hinders the continuation of the process. This would result in a severe reduction of the film formation rate. However, breakdown of this layer takes place and pores nucleate after that over the entire surface. Pores then grow by a localized field-assisted dissolution mechanism, injecting Al(III) cations directly into the solution by effect of the electric field at the bottom of the pores. At this point, the system stabilizes and "stationary" conditions are attained since the two competitive processes are compensated themselves: oxide formation at the metal/oxide interface and field-assisted chemical etching of the alumina at the bottom of the pores, generating the two-layered structure. Stationary conditions are not maintained indefinitely, since the porous layer gets thicker with time. This can alter the growth mechanism of the layer if anodising times are too long in a way that may cause alterations on the final structure [14,15].

Several works devoted to the synthesis of semiconducting materials arrays report the use of either commercial or home-made AAMs. The latter presents the advantage of tuning the pore size from few nanometers to hundreds of nanometers by tailoring the anodising conditions. Among the strategies followed for filling the pores of the AAMs templates, the electrochemical deposition and sol–gel based methods are being largely exploited [16–27].

However, information regarding the thermal stability of AAMs lacks. As-prepared AAMs are amorphous and contain anions from

* Corresponding author at: Institut Català de Nanotecnologia, Campus de la UAB, E-08193 Bellaterra, Spain. Tel.: +34 935814923; fax: +34 935814747.
E-mail address: Eva.Pellicer.icn@uab.cat (E. Pellicer).

0254-0584/$ – see front matter © 2008 Elsevier B.V. All rights reserved.
doi:10.1016/j.matchemphys.2008.05.003

the electrolyte but they can be converted to polycrystalline. Annealing of the AAMs in air brings changes in their structure, as well as changes in the concentration and composition of the impurities. Moreover, the annealing process is expected to increase the chemical resistance and stability at high temperatures. In this sense, it was reported that thermally treated AAMs showed higher corrosion resistance both in alkaline and acid media [28]. Besides, it has been described that annealing processes induce changes in the photoluminescence properties of AAMs [29].

The knowledge of how AAMs behave when performing heat-treatments has a twofold interest. On the one hand, mineralization or oxidation of the precursors is often needed for yielding the desired semiconducting materials. On the other hand, structural applications such as gas sensor devices involving anodic alumina as the supporting platforms are subjected to high temperatures (up to 900 °C or even higher) enabling gas sensing. Moreover, temperature of the sensor is sometimes periodically pulsed for improving sensor performance.

In this work, the thermal stability of AAMs is addressed by means of characterization of their morphology by scanning electron microscopy (SEM) and their structure by X-ray diffraction (XRD). For this purpose, the materials are subjected to different thermal treatments in order to assess final membrane appearance and to investigate if significant structural changes occur. Laminated 1050 aluminium alloy (99.5%) is anodised instead of ultra pure aluminium (99.999%), commonly used by numerous researchers, making the whole process more economical. However, this alloy contains intermetallic compounds and this fact must be taken into account when analyzing the results, as it can affect the structure of the AAM. In addition, the influence of the barrier layer on the mechanical and thermal stability of the AAMs is presented for the first time. Membranes are prepared both with and without chemical removing treatment of the barrier layer.

2. Experimental

AAMs were obtained using as-received commercial sheets of laminated AA1050 (99.5% purity, 30 mm × 30 mm × 0.7 mm). As described elsewhere [30,31], optimal surfaces for anodisation were obtained by a four-step process: aluminium sheets were degreased with an industrial degreaser (Metex T5-40A, from McDermid Inc.), etched in an alkaline solution (5% NaOH, 3% sodium gluconate), desmutted in 30% HNO_3, electropolished in a H_3PO_4:H_2SO_4 3:2 bath for 10 min at 150 mA cm^{-2} and finally etched in a 3.5% H_3PO_4: 2% CrO_3 solution for 10 min. Without delay, a single-step potentiostatic anodising at 45 V was carried out in a 0.30-M oxalic acid electrolyte at 20 ± 0.2 °C for 1 h. Anodising was conducted in a thermostatized two-electrode cell containing a lead cathode and vigorously agitated by air. Temperature was regulated by a Polyscience cryostat (model 9106) and a power supply from GRELCO Inc. (model GE2501DVG) was used to apply voltage to the cell (max. 250 V–1 A). Preparation of AAMs was performed by a chemical etching procedure which included five steps. As samples were both-side anodised, firstly one side was protected with a lacquer. The unprotected anodised side was etched in a concentrated NaOH solution. Then the exposed aluminium substrate was removed by a $CuCl_2$:HCl 1.2:20% solution. The AAM was optionally etched in a 2% H_3PO_4 solution at 35 °C for 60 min to eliminate the barrier layer. In this step, etching time is an important parameter to control and is related to the voltage applied during anodising [30]. Finally, acetone was used to remove the lacquer and samples were rinsed with twice distilled water and stored in vacuum. All solutions used in this work were prepared with analytical grade reagents and twice distilled water.

As-synthesized AAMs were annealed in a muffle under atmospheric conditions. Five replicas of each sample were heat treated under controlled conditions to ensure reproducible results. First, a linear heating sweep from room temperature to the selected final temperature (T_s) was applied with a rate of 1 °C min^{-1}. Then, the temperature T_s was held constant for 4 h and samples were cooled down inside the muffle till room temperature.

XRD analyses were performed on a Panalytical diffractometer working with the Cu Kα radiation (λ = 1.5418 Å). Diffractograms were obtained in the 4–100° 2θ range with a step range of 0.05° and a holding time of 5 s per step.

The on-top and on-bottom structure of the porous AAM was analyzed by field emission scanning electron microscopy (FE-SEM Hitachi H-4100FE), after sputtering a thin conductive carbon layer on the surface. Cell diameters from the AAMs were then estimated by statistical calculations from SEM images [31].

3. Results and discussion

Fig. 1 shows the on-top and on-bottom morphology of as-synthesized AAMs. One can observe a pore array distribution on-top (Fig. 1a), while the on-bottom morphology was typical of an alumina barrier film (Fig. 1b, left). The removal of the barrier film in aqueous phosphoric acid allowed the pore bottoms to open (Fig. 1b, right), so that a honeycomb porous structure appeared with no lateral crossovers between individual pores. This etching process also led to some pore widening. Note that the anodising parameters used yielded membrane thicknesses ranging from 15 to 20 μm and pore diameters about 20 nm on-top. The barrier layer was of the order of few nanometers. Intermetallic compounds (IMCs) in AA1050, mainly Al–Fe–Si and Al–Si, have influence on the anodising process [32]. These particles show a chemical dissolution rate and an electrochemical oxidation rate lower than in bulk aluminium. This may cause local destructuration of the AAM when incorporated to it. Pretreatment mainly minimizes the amount of these particles over the surface, but nothing can be done to eliminate the inner IMCs. So, the longer the anodising is, the more defects in the AAM appear. That is the reason why anodising is carried out only for 1 h. Anyway, the quality of the porous alumina films was found to be reasonably good provided that impure aluminium foil was anodised. Actually, it was recently reported that the chemical composition of alumina membranes obtained from either impure or ultra pure foils is very similar [33]. However, the same authors observed that alumina membranes synthesized from impure aluminium contained smaller pore sizes with a larger size distribution, though these qualities improved upon annealing.

After checking the AAMs morphology, specimens were annealed in air to assess their final appearance from a qualitative point of view. T_S values were chosen according to previous data found in the

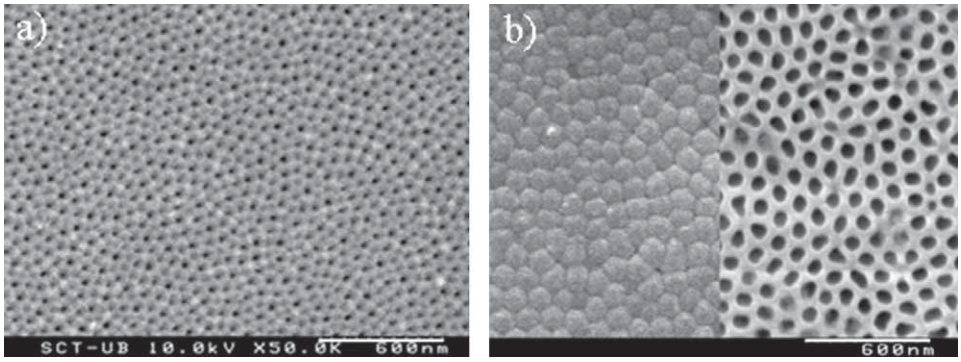

Fig. 1. On-top (a) and on-bottom (b) with barrier layer (left) and without barrier layer (right) views of as-synthesized AAMs.

literature. Routkevitch et al. [12] reported the formation of γ-Al_2O_3 in the first crystallization step of anodic alumina prepared from oxalic-based solutions around 830 °C. Successive transformations provided δ- and α-Al_2O_3. Other authors reported the transformation of as-prepared amorphous alumina from oxalic solutions to γ-Al_2O_3 at 600 °C for 4 h [34]. Akahori [35] pointed out that the melting point of the barrier layer was lower than that of the bulk alumina (1000 °C instead of 2017 °C), which made the melting point of porous anodic alumina to be around 1000 °C. In this work, we applied the following temperatures: 750, 900, 1000 and 1100 °C.

As refers to the mechanical deformation caused by the thermal treatment, it was observed that the AAMs without the barrier layer suffered from bending when annealed at T_s higher than 750 °C. By contrast, the ones keeping the barrier layer did not bend or they got slightly wrinkled. This fact pointed out that the barrier layer mechanically stabilized the porous layer from the thermal dilatation.

In order to minimize the bending effect, as-synthesized AAMs with 13 g load on top were placed into the muffle and annealed. The samples were initially heated up to T_s = 1100 °C and afterwards subjected to several heat-treatments at lower temperatures. The AAMs with the load on top showed less creases than the load-free ones as long as they had barrier layer. Once the first heat-treatment had been performed, no further changes were observed in subsequent thermal treatments at the same (or lower) temperatures and even with no weight put onto the samples. By contrast, AAMs without compact layer broke during the annealing if load was used (Fig. 2).

The occurrence of structural changes as a result of the long-term heat-treatments was analyzed by designing a systematic X-ray diffraction study. As-prepared AAMs were amorphous and no transformations were observed after annealing at 750 °C (Fig. 3). This result was in agreement with previous works [36–38] in which high purity aluminium (99.999%) was used, while Chen et al. reported the formation of γ-Al_2O_3 after annealing at 600 °C of a single-step anodised commercial aluminium (99.7%) [34]. The diffractograms of samples annealed at T_s = 900 °C are displayed in Fig. 4, along with the corresponding heat-treatment cycle applied. As can be seen, crystallization occurred in AAMs to some extent. Two main peaks placed at 45.8 and 67.0 2θ were observed in the diffractograms. The one located at higher angle can be assigned to the (4 4 0) reflection of γ-Al_2O_3 (JCPDS cards nos. 47-1308 and 29-0063), while the one located at lower angle can be assigned to the (4 0 0) reflection of the same phase. We, therefore, assumed that γ-Al_2O_3 was mainly formed at this temperature and this was in agreement with previous data reported in the literature [37]. A careful comparison of

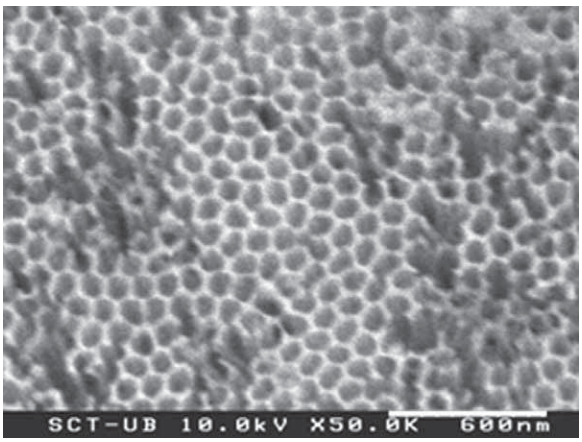

Fig. 2. SEM image of an AMM without barrier layer heat treated at 1100 °C. Cracks are visible even at the nanometer scale.

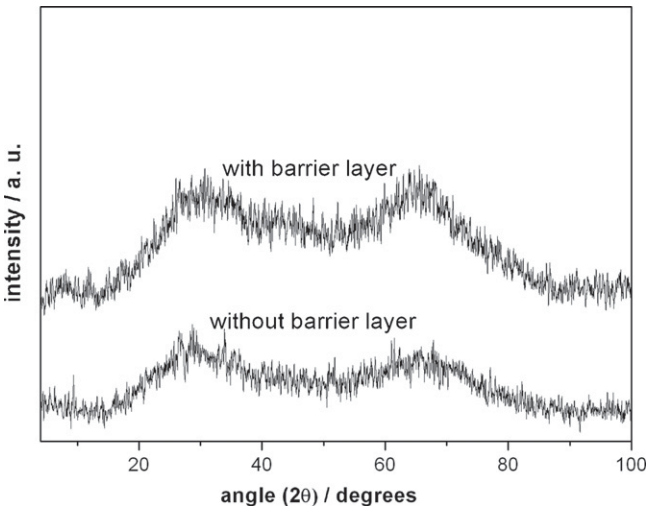

Fig. 3. X-ray diffractograms of AAMs with and without barrier layer after heat-treatment at 750 °C.

the XRD patterns for AAMs calcined at T_s = 1100 °C shed light on the temperature-induced structural transitions of the barrier layer (Fig. 5). Peaks labelled as (*) in Fig. 5 were attributed to the crystallization of the inner layer and belong to the α-Al_2O_3 phase, while the rest of the peaks corresponded to the porous layer and were mainly assigned to γ-Al_2O_3. Although the formation of α-Al_2O_3 was expected at a temperature above 1100 °C [36,39,40], the present data demonstrate that it is possible to achieve this phase at lower temperature. In fact, the coexistence of γ and α phases was reported in Cr^{3+} doped AAMs annealed at 800 °C and the existence of a very

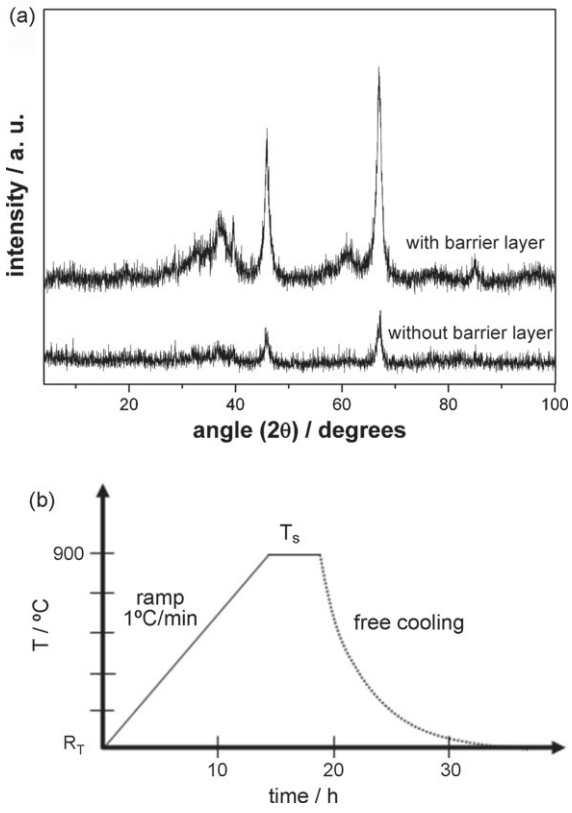

Fig. 4. (a) X-ray diffractograms of AAMs with and without barrier layer after heat-treatment at 900 °C. (b) Scheme of the heat-treatment cycle used.

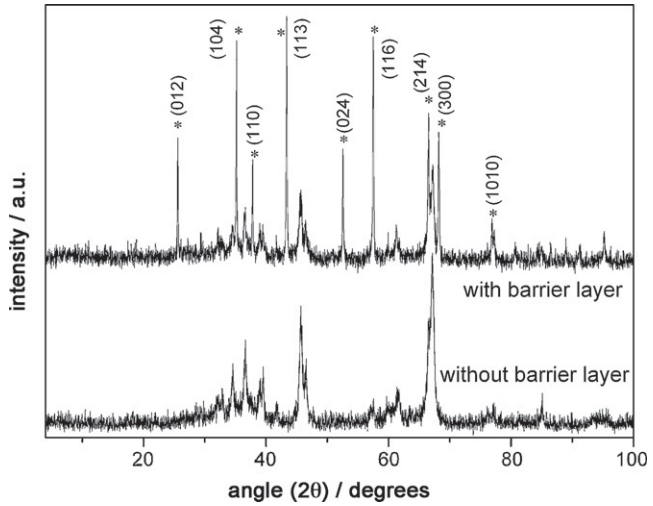

Fig. 5. X-ray diffractograms of AAMs with and without barrier layer after heat-treatment at 1100 °C. (*) Peaks belong to the barrier layer.

pure α-Al_2O_3 was detected at 1000 °C [38]. It is worth mentioning that now it can be assured that the formation of the α phase was due to the presence of the barrier layer since this phase was not detected in the inner layer-free membranes.

The Scherrer's formula was used to estimate the average grain size from the main diffraction peaks (1):

$$D = \frac{K\lambda}{\beta \cos\theta} \quad (1)$$

where β is the full width at half maximum of the peak and D is the particle diameter. Under our experimental conditions, $K = 0.9$ and λ is Kα Cu wavelength (1.1548 Å). Table 1 summarizes the estimated grain size of AAMs with and without barrier layer as a function of the annealing temperature.

For those samples without barrier layer, the grain size slightly increased with T_s from ~10 nm to 20–25 nm. The increase was noticeable when going from 1000 to 1100 °C. This trend was also observed in the AAMs preserving the inner layer if we only take into account the diffraction peaks clearly attributed to pore walls re-crystallization. By contrast, larger grain sizes (around 80 nm) were obtained from the peaks associated with the inner layer crystallization at 1100 °C. This fact was interpreted as an effect of the porous structure in the outer layer. Pores could in fact hinder the growth of alumina crystals, while in the barrier layer such obstacles were not affecting their growth.

Table 1
Grain size estimated using Scherrer's formula for AAMs with and without barrier layer

T_s (°C)	2θ (°)	AAM with barrier layer, D (nm)	AAM without barrier layer, D (nm)
900	45.8	10.2	8.9
	67.0	11.2	10.5
1000	45.8	12.6	12.3
	67.0	11.1	11.8
1100	25.6[a]	87.3	–
	34.6	18.3	27.7
	35.2[a]	86.6	–
	36.6	27.4	24.3
	43.4[a]	88.4	–
	45.7	18.2	19.3
	57.5[a]	71.9	–
	67.1	22.1	19.0

[a] Peaks belong to the barrier layer.

It was observed qualitatively that the AAM size increased with the first structural change (from amorphous alumina at room temperature to polycrystalline alumina at 900 °C). Further phase transitions did not bring appreciable changes in size. In order to clarify the effect of heat-treatments in the structure of AAMs, SEM images of on-top and on-bottom morphology were taken and a statistical calculation based on the cell parameters was made.

Fig. 6 shows the morphology in both sides of the AAMs that resulted after single anodising in oxalic acid and membrane preparation procedure involving eventual barrier layer elimination. The calculated cell diameter is depicted in each image. Similar values of cell parameters and comparable hexagonal arrangements were obtained in the bottom side of the AAMs (Figs. 6c and d), independently of pores being closed by the barrier layer. However, on-top pore densities in samples with barrier layer were higher than in samples where the barrier layer had been removed (Figs. 6a and b) and thus, a lower cell density was found. This fact was explained as a consequence of the initial steps of the anodising process. In AAMs generated by single-step anodising, more than one pore initially nucleate by each cell. Nucleation is not a homogeneous process and takes place generating disordered structures. Moreover, initial surface condition has a great influence on these steps. That is the reason why two-step anodising is applied when ordered structures are desired by this method [30,41,42]. After nucleation, pores in a cell combined underneath or just some terminated and a ratio of one pore per cell with a cell diameter related to the applied voltage was then found [31,42]. This was seen in the on-bottom structure and resulted in greater cell diameters. During the chemical etching step of the barrier layer, the solution filled the pores once the barrier layer was dissolved. As a result, the cell walls were etched and these initial pores in the on-top surface tended to unify. Thus, similar pore densities were obtained in the on-top and on-bottom structures when the barrier layer had been removed (Fig. 6b and d). This was very similar to the effect that pore-widening treatments commonly used produced in the on-top morphology.

Albeit nanopore arrays did not collapse on the surface during the annealing, even at T_s = 1100 °C, a progressive change in the AAM morphology was observed.

Regarding the samples without barrier layer, it was observed that the cell diameter increased with T_s between 900 and 1000 °C (Fig. 7). This was caused by the dilatation of the pore wall, which was clearly visible in the on-top surface. This change was in agreement with the furthest crystallization of AAMs seen in X-ray experiments. As a consequence of pore wall dilatation, cracking at the nanometer scale also appeared. Another effect was the disordering of the pore array. Less consistent results were obtained in the on-bottom structure because the barrier layer etching treatment affected the pore wall thickness and this phenomenon was not as clear as in the on-top surface.

Same experiments were performed in samples with barrier layer. On-top cell diameter drastically increased after heat-treatment at 1000 °C (see Figs. 6a and 8a) and a value equal to the on-bottom cell diameter was found (compare Figs. 6c and 8b). This phenomenon was attributed to the degradation of the pore nucleation layer above described. Dilatation of the cell walls was also observed and more disordered structures were obtained, the same behaviour that showed AAMs without barrier layer. Concerning the effect of heat-treatments to the barrier layer, the dilatation of cell walls was not observed in this case but a gradual transparency in SEM views of the layer appeared (Fig. 8b), probably related to the crystallization of the layer. It is worth highlighting that cracking at the nanometer scale was not observed at both sides of these sam-

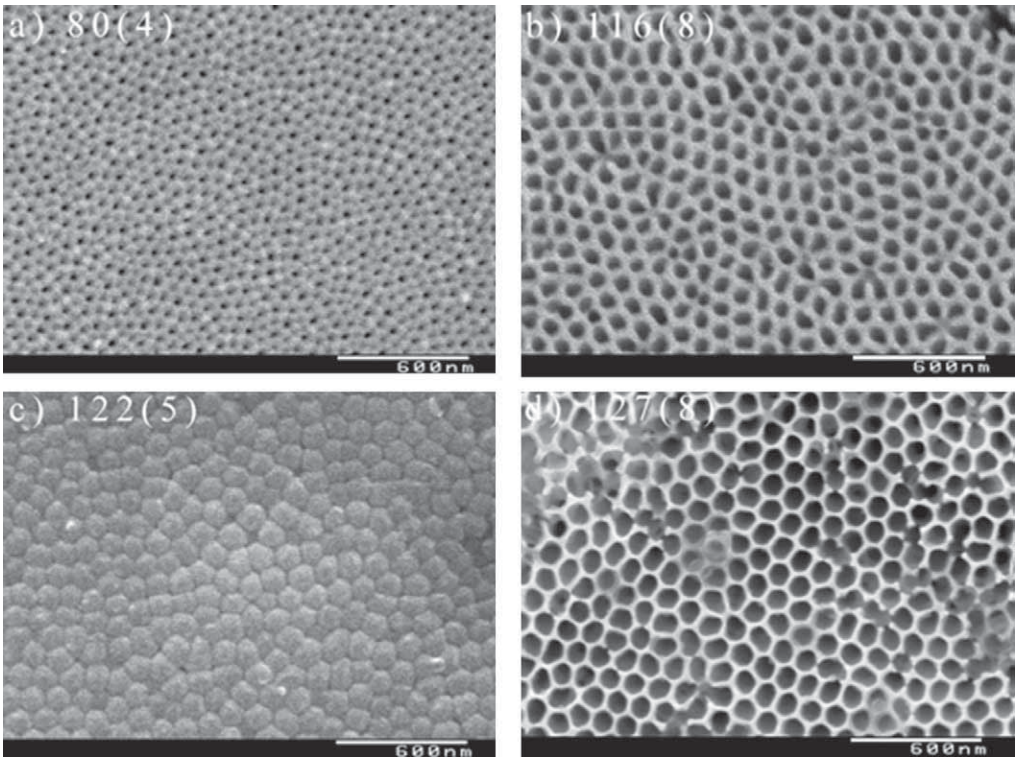

Fig. 6. SEM images of on-top (a) and on-bottom (c) as-synthesized AAMs without barrier layer removing; on-top (b) and on-bottom (d) views of samples subjected to barrier layer etching treatment. The given numbers correspond to the calculated cell diameter or interpore distance (nm) and the estimated error of the measure (in brackets).

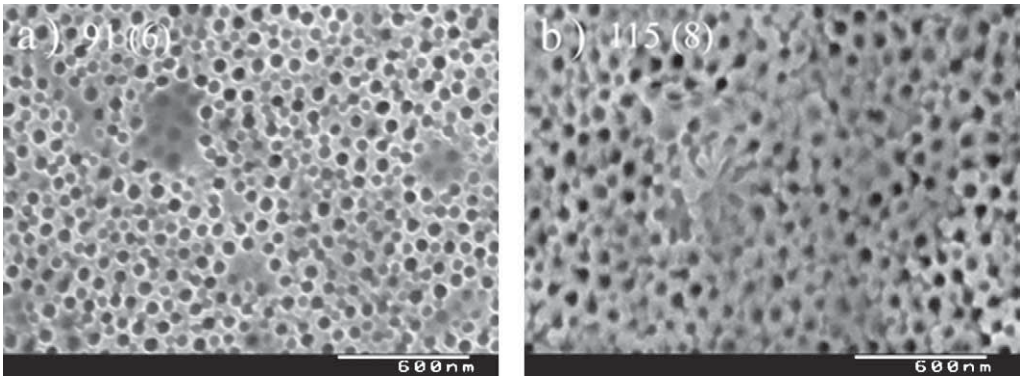

Fig. 7. SEM images of on-top surface of AAMs without barrier layer after heat-treatment at (a) 900 °C and (b) 1000 °C. The given numbers correspond to the calculated cell diameter or interpore distance (nm) and the estimated error of the measure (in brackets).

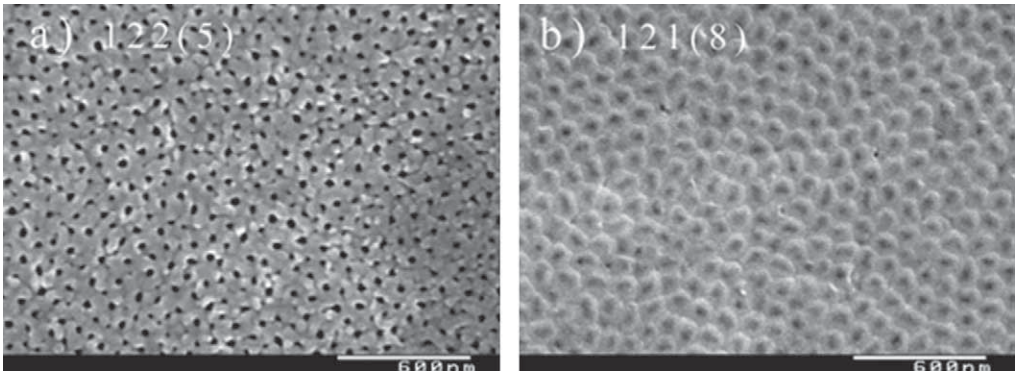

Fig. 8. SEM images of (a) on-top and (b) on-bottom surface of AAMs with the barrier layer after heat-treatment at 1000 °C. The given numbers correspond to the calculated cell diameter or interpore distance (nm) and the estimated error of the measure (in brackets).

ples, pointing out the thermal and mechanical stabilizing effect that the barrier layer gives to the AAMs.

4. Conclusions

In this work, the thermal stability of AAMs is explored. The compact layer provides high stability to AAMs, in spite of its small thickness (few nanometers). An eventual barrier layer removal is harmful, since bending or cracking occurs upon annealing. The pore arrays are maintained after annealing at high temperatures (up to 1100 °C), even though the morphology slightly changes. A clear re-crystallization of the barrier layer in the α-Al_2O_3 phase has been detected by means of XRD analyses after annealing at 1100 °C. Barrier layer re-crystallization results in larger grain sizes than those corresponding to the porous layer. A statistical estimation based on cell density values unveiled on-top cell wall dilation in AAMs without barrier layer. This resulted in sample cracking. Dilatation was also observed in on-top AAMs with barrier layer but, in this case membrane cracking was avoided. Thus, it is advisable to keep the barrier layer in those applications requiring stability to thermal shocks or remove it once an appropriate thermal treatment is performed.

Acknowledgments

This work was supported by MAT 2004-06859-C02-01 and MAT 2006-12913-C02-01 projects, both from the *Comisión Interministerial de Ciencia y Tecnología* (CICYT). The authors thank the Serveis Cientificotècnics of the University of Barcelona for the equipment facilities. EME is with CeRMAE, center on Advanced Materials for Energy of the Generalitat de Catalunya. Both EME and Electrodep belong to IN2UB (Institut de Nanociència i Nanotecnologia de la Universitat de Barcelona). J. M. Montero also thanks the DURSI and the European funds for their financial support.

References

[1] E. Schofield, Trans. Inst. Met. Finish. 83 (2005) 35.
[2] G.Q. Ding, M.J. Zheng, W.L. Xu, W.Z. Shen, Nanotechnology 16 (2005) 1285.
[3] C.-S. Toh, B.M. Kayes, E.J. Nemanick, N.S. Lewis, Nano Lett. 4 (2004) 767.
[4] Z. Wu, C. Richter, L. Menon, J. Electrochem. Soc. 154 (2007) E8.
[5] F. Li, L. Zhang, R.M. Metzger, Chem. Mater. 10 (1998) 470.
[6] A.P. Li, F. Müller, A. Birner, K. Nielsch, U. Gösele, J. Appl. Phys. 84 (1998) 6023.
[7] G.E. Thompson, Thin Solid Films 297 (1997) 192.
[8] N.V. Myung, J. Lim, J.-P. Fleurial, M. Yun, W. West, D. Choi, Nanotechnology 15 (2004) 833.
[9] A. Cai, H. Zhang, H. Hua, Z. Zhang, Nanotechnology 13 (2002) 627.
[10] D. Crouse, Y.-H. Lo, A.E. Miller, M. Crouse, Appl. Phys. Lett. 76 (2000) 49.
[11] A. Govyadinov, P. Mardilovich, K. Novogradecz, S. Hooker, D. Routkevich, Proceedings of the ASME Int. Mechanical Engineering Congress, MEMS, vol. 2, Orlando (Florida), 2000, pp. 313–318.
[12] D. Routkevitch, A.N. Govyadinov, P.P. Mardilovich, Proceedings of the ASME Int. Mechanical Engineering Congress, MEMS, vol. 2, Orlando (Florida), 2000, pp. 39–44.
[13] P.G. Sheasby, R. Pinner, The Surface Treatment and Finishing of Aluminium and its Alloys, 6th ed., Finishing Publications Ltd. with ASM International, USA, 2001.
[14] M. Nagayama, K. Tamura, Electrochim. Acta 13 (1968) 1773.
[15] P.-S. Wei, T.-S. Shih, J. Electrochem. Soc. 154 (2007) C678.
[16] M. Zheng, G. Li, X. Zhang, S. Huang, Y. Lei, L. Zhang, Chem. Mater. 13 (2001) 3859.
[17] A. Kolmakov, Y. Zhang, M. Moskovits, Nano Lett. 3 (2003) 1125.
[18] X. Zhang, Y. Hao, G. Meng, L. Zhang, J. Electrochem. Soc. 152 (2005) C664.
[19] S. Gavrilov, L. Nosova, I. Sieber, A. Belaidi, L. Dloczik, Th. Dittrich, Phys. Stat. Sol. A 202 (2005) 1497.
[20] Q. Wang, G. Wang, B. Xu, J. Jie, X. Han, G. Li, Q. Li, J.G. Hou, Mater. Lett. 59 (2005) 1378.
[21] Y. Lin, G.S. Wu, X.Y. Yuan, T. Xie, L.D. Zhang, J. Phys.: Condens. Matter 15 (2003) 2917.
[22] C. Goh, K.M. Coakley, M.D. McGehee, Nano Lett. 5 (2005) 1545.
[23] A. Huczko, Appl. Phys. A 70 (2000) 365.
[24] M. Hernandez-Velez, Thin Solid Films 495 (2005) 51.
[25] J.C. Hulteen, C.R. Martin, J. Mater. Chem. 7 (1997) 1075.
[26] S. Inoue, S.Z. Chu, K. Wada, D. Li, H. Haneda, Sci. Technol. Adv. Mater. 4 (2003) 269.
[27] C.Y. Han, Z.L. Xiao, H.H. Wang, G.A. Willing, U. Geiser, U. Welp, W.K. Kwok, S.D. Bader, G.W. Crabtree, Plat. Surf. Finish. 91 (2004) 40.
[28] C.W. Lee, H.S. Kang, Y.H. Chang, Y.M. Hahm, Korean J. Chem. Eng. 17 (2000) 266.
[29] J.H. Wu, X.L. Wu, N. Tang, Y.F. Mei, X.M. Bao, Appl. Phys. A 72 (2001) 735.
[30] J.M. Montero-Moreno, M. Sarret, C. Müller, Surf. Coat. Technol. 201 (2007) 6352.
[31] J.M. Montero-Moreno, M. Sarret, C. Müller, J. Electrochem. Soc. 154 (2007) C169–C174.
[32] J.M. Montero-Moreno, M. Sarret, C. Müller, in preparation.
[33] D. Lo, R.A. Budiman, J. Electrochem. Soc. 154 (2007) C60.
[34] C.C. Chen, J.H. Chen, C.G. Chao, Jpn. J. Appl. Phys. 44 (2005) 1529.
[35] H. Akahori, J. Electron. Microsc. Jpn. 11 (1962) 217.
[36] M.E. Mata-Zamora, J.M. Saniger, Rev. Mex. Fis. 51 (2005) 502.
[37] X. Sun, F. Xu, Z. Li, W. Zhang, J. Lumin. 121 (2006) 588.
[38] T. Li, S. Yang, L. Huang, J. Zhang, B. Gu, Y. Du, J. Phys.: Condens. Matter 16 (2004) 2463.
[39] P.P. Mardilovich, A.N. Govyadinov, N.I. Mukhurov, A.M. Rzhevskii, R. Paterson, J. Membr. Sci. 98 (1995) 131.
[40] R. Ozao, M. Ochiai, N. Ichimura, H. Takahashi, T. Inada, Thermochim. Acta 352/353 (2000) 91.
[41] H. Masuda, K. Fukuda, Science 268 (1995) 1466.
[42] G.D. Sulka, S. Stroobants, V. Moshchalkov, G. Borghs, J.-P. Celis, J. Electrochem. Soc. 149 (2002) D97.